Thesis for Master of Science Degree in Molecular Biosciences

The regulation of Gb3 biosynthesis in cancer cells: Implications for membrane dynamics

Simona Lukoševičiūtė

Department of Molecular Biosciences
The Faculty of Mathematics and Natural Sciences
UNIVERSITY OF OSLO

May 2011

The important thing in science is not so much to obtain new facts as to discover new ways of thinking about them.

William Lawrence Bragg

Acknowledgement

The present work was carried out from April 2010 to May 2011 in the group of Professor Kirsten Sandvig at the Department of Biochemistry, Institute for Cancer Research at the Norwegian Radium Hospital.

First I would like to express my sincere gratitude to Professor Kirsten Sandvig for the opportunity to work in her group, and for her exceptional expertise and guidance I have received throughout this work. I am also very thankful to the whole group who all were helpful and friendly to me.

I would like to give exceptional thanks to Jonas Bergan and Tore Skotland for the critical reading of my thesis and their useful feedback. I received valuable teaching and guidance from Anne Grethe Myrann during my first steps in the new lab, and I am highly grateful to her for this. I would also like to acknowledge Angela Oppelt who helped me a lot with the cell migration assay.

I am grateful to everyone in the Department of Biochemistry for a warm and supportive working environment, and I want to give special thanks to Ieva, Nagham, Audun, Carl-Martin, Santosh, Anne-Mari and Jane for all cheerful moments we had in the lab. Additionally, I am very thankful to my friends Zivile and Kotryna who shared their time and thoughts with me during our jolly lunch brakes.

I am also extremely grateful to my friend and employer Petras Juzenas who invited me to his group two year ago and gave me the opportunity to work and study here in Oslo.

Finally, I would like to thank my fiancé Arturas for his love and strength during the most difficult moments. I would never have accomplished this without you!

My sincere thanks go to everyone reading this, because this is what I have been working on for the past year. I hope you will enjoy it!

Table of Content

Abbreviations

2DG	2-deoxy-D-glucose
BSA	Bovine serum albumin
IC_{50}	Concentration of a toxin which inhibits protein synthesis by 50%
cDNA	Complementary DNA
DMEM	Dulbecco's modified Eagle's medium
DRM	Detergent resistant membrane domain
DT	Diphtheria toxin
EDTA	Ethylenediaminetetraacetic acid
ER	Endoplasmic reticulum
FBS	Fetal bovine serum
Gb3	Globotriaosylceramide
Gb3syn	Gb3 synthase gene
GSL	Glycosphingolipid
HUS	Haemolytic uremic syndrome
MESNa	Sodium 2-mercaptoethanesulfonate
PBS	Phosphate buffered saline
PDMP	DL-threo-1-phenyl-2-decanoylamino-3-morpholino-1-propanol
PCR	Polymerase chain reaction
qRT-PCR	Quantitative real time reverse transcription polymerase chain reaction
RPMI	Medium developed by Moore *et al.* at Roswell Park Memorial Institute
RT	Room temperature
RT-PCR	Reverse transcription polymerase chain reaction
SEM	Standard error of the mean
SLT	Shiga-like toxin
Stx	Shiga toxin
StxB-sulf2	A modified B-moiety of Stx containing two sulfation sites
TBP	TATA-binding protein
TCA	Trichloroacetic acid

Abstract

Gb3 (Gal α1-4, Gal β1-4, Glc β1-1, Ceramide) is a neutral glycosphingolipid specifically expressed in several human tissues, and is recognised as a receptor for Shiga toxins. Gb3 has been demonstrated to be upregulated in a number of cancer types [1], which makes it a feasible target for cancer diagnosis and therapy. However, little is known about the regulation of Gb3 biosynthesis in the cells, and further investigations are needed. In this study, a quantitative real time RT-PCR technique was used to investigate the changes in Gb3 synthase gene (Gb3syn) expression in several cancer cell lines. We demonstrated that Gb3syn expression was upregulated in response to higher cell density and longer culturing time in HEp-2 cells, while no regulation was detected in other cell lines tested. The effects of two Gb3 synthesis modulating compounds, 2-deoxy-D-glucose (2DG) and sodium butyrate, were also studied. 2DG inhibited the expression of Gb3syn in HEp-2 cells and induced cell protection against Shiga toxin (Stx) and diphtheria toxin (DT). The binding and endocytosis of Stx was not affected by 2DG, and cell sensitivity to Stx was not rescued by pyruvate indicating that the protection observed after 2DG treatment was not due to lack of ATP. Thus it was concluded that later steps of intoxication by Stx, retrograde transport to the Golgi apparatus and the endoplasmic reticulum and/or translocation to the cytosol, were perturbed by 2DG-treatment and led to cell protection against the toxin. In contrast, sodium butyrate upregulated Gb3syn expression in colon cancer cells, and increased their sensitivity to Stx. The data indicated that two distinct mechanisms, changed intracellular transport and/or higher binding of the toxins, were responsible for cell sensitisation by sodium butyrate. Finally, the relation between Gb3 and cancer cell metastatic potential was studied using a live time-lapse imaging combined with immunofluorescence microscopy, which allowed us to analyse individual cells. The preliminary data suggest that there is a correlation between Gb3 exposed on the plasma membrane and the motility of cancer cells.

Aim of the study

Gb3 is a neutral glycosphingolipid specifically expressed in several human tissues with the highest levels present in kidneys [2-4], microvascular endothelium [5;6] and platelets [7]. Gb3 serves as a receptor for several protein toxins, such as Shiga toxin and ricin, and also has been found to be over-expressed in numerous cancer types [1]. Moreover, several studies have indicated a relation between the expression of Gb3 and cancer metastasis [8;9], thus making Gb3 a feasible target for cancer diagnosis and therapy. However, little is known about the regulation of Gb3 synthesis in the cells. An increased knowledge about Gb3 expression may help to understand the development and progression of cancer, and thereby suggest new ways for cancer diagnosis and treatment.

The first part of this study was focused on the regulation of Gb3 synthesis in cancer cells. We studied expression of the Gb3 synthase gene (Gb3syn) in several cancer cell lines, and investigated changes induced by two Gb3 synthesis modulating compounds, 2-deoxy-D-glucose (2DG) and sodium butyrate. To investigate the consequences of altered expression of Gb3syn and the associated changes in cellular Gb3, we used Shiga toxin and other protein toxins to study the levels of Gb3 available for ligand binding. Furthermore, changes in cell sensitivity to these toxins allowed us to predict molecular effects provoked by 2DG and sodium butyrate in cancer cells.

In the second part of the study, we investigated a possible relationship between Gb3 and metastatic potential of cancer cells. Furthermore, since the level of detectable Gb3 had been shown to vary dramatically not only between different cell types, but also within the same cell culture, a method based on individual cell analysis was needed. Therefore, we combined two methods, the continuous phase contrast imaging followed by the conventional immunofluorescence microscopy. This approach allowed us to study a direct correlation between migratory capacity and the cellular Gb3 of an individual cell.

1. Introduction

1.1. Sphingolipids

Sphingolipids are a diverse group of lipids sharing a common backbone structure consisting of a fatty acid chain linked via an amide bond to a long-chain aliphatic base – sphingoid (Fig. 1.1). Sphingolipids have longer and more saturated hydrocarbon chains than other membrane lipids, and thus they are thought to accumulate in specialized transient cholesterol-rich membrane domains called lipid rafts [10]. However, due to their nano-scale size and dynamicity, lipid rafts are difficult to study. Most of the studies on lipid rafts are based on detergent extraction and/or labelling with multivalent ligands which may cause redistribution and clustering of specific lipids [11]. Therefore, there is still an ongoing debate about the existence and functions of lipid rafts in natural biological membranes. However, the controversies in the field inspired new efforts, and advanced microscoping techniques, which can go beyond the diffraction limit, and improved lipidome analysis are now being employed in the field [12].

1.1.1. Synthesis and metabolism

The simplest sphingolipid, ceramide, serves as a key intermediate molecule for the synthesis of complex sphingolipids. Ceramide can be synthesised *de novo* from serine and fatty acids – fatty acids enter the reaction bound to coenzyme A (FA-CoA) (Fig. 1.1). Ceramide can also be rapidly formed by the breakdown of more complex sphingolipids, such as sphingomyelin [13]. *De novo* synthesis of ceramide occurs on the cytosolic side of the endoplasmic reticulum (ER) and possibly in ER-associated membranes such as the perinuclear membrane [14]. However, more complex sphingolipids and glycosphingolipids are synthesised in the Golgi, and thus ceramide needs to be transported between the ER and the Golgi (Fig. 1.2). Two distinct pathways have been revealed for ceramide transport from the ER to the Golgi: (i) non-vesicular transport by ceramide transfer protein CERT and (ii) vesicular transport. The CERT-mediated transport of ceramide has been shown to deliver ceramide specifically for the synthesis of sphingomyelin, while *de novo* glycosphingolipid synthesis in the Golgi has been suggested to be CERT-transport independent [15].

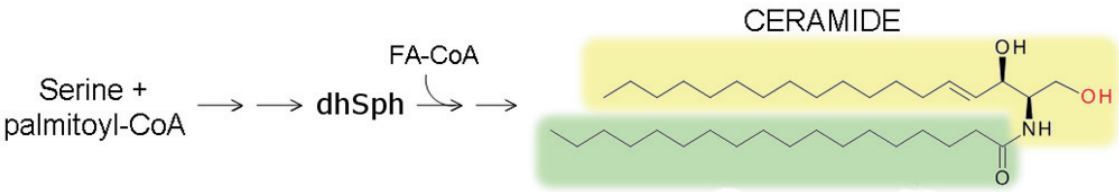

Fig. 1.1. *De novo* biosynthesis of ceramide. During the first two reactions, dihydrosphingosine (dhSph) is synthesised from serine and palmitic acid (C16:0). The dhSph is then N-acylated by fatty acyl-CoA (FA-CoA) to form dihydroceramide (not shown). Finally, the dhSph part of the dihydroceramide is desaturated in the position 4,5 and ceramide is formed. The sphingosine is depicted in yellow, and the fatty acyl chain is marked in green (here shown as C18:0) in the structure of the ceramide. More complex sphingolipids can be synthesised by the addition of head groups such as carbohydrates (glycosphingolipids) or phosphocholine (sphingomyelin) to the ceramide backbone. The head groups of complex sphingolipids are linked via the hydroxyl group shown in red.

1.1.2. Glycosphingolipids

Glycosphingolipids (GSLs) share a common backbone structure (ceramide) with other sphingolipids, but are distinguished from the rest by carbohydrates attached to the terminal hydroxyl group of the ceramide [16]. Monoglycosylceramides, GSLs containing a single sugar molecule, are synthesized by a direct transfer of the carbohydrate moiety from a sugar-nucleotide, e.g. uridine 5-biphosphate(UDP)-galactose or UDP-glucose, to ceramide [13]. The galactosylation and glycosylation of ceramide take place in two different compartments of the cell: galactosylceramide (GalCer) is synthesized on the luminal side of the ER membrane, while glucosylceramide (GluCer) is synthesized on the cytosolic surface of the Golgi membrane [11]. GluCer, which is the precursor of the majority of GSLs in the cells, is translocated to the lumen of the Golgi where the synthesis of more complex GSLs occurs [14] (Fig. 1.2). GluCer is then converted to lactosylceramide (LacCer) by the addition of one galactose residue, and it is then further glycosylated to more complex GSLs [11] as shown in Fig. 1.3.

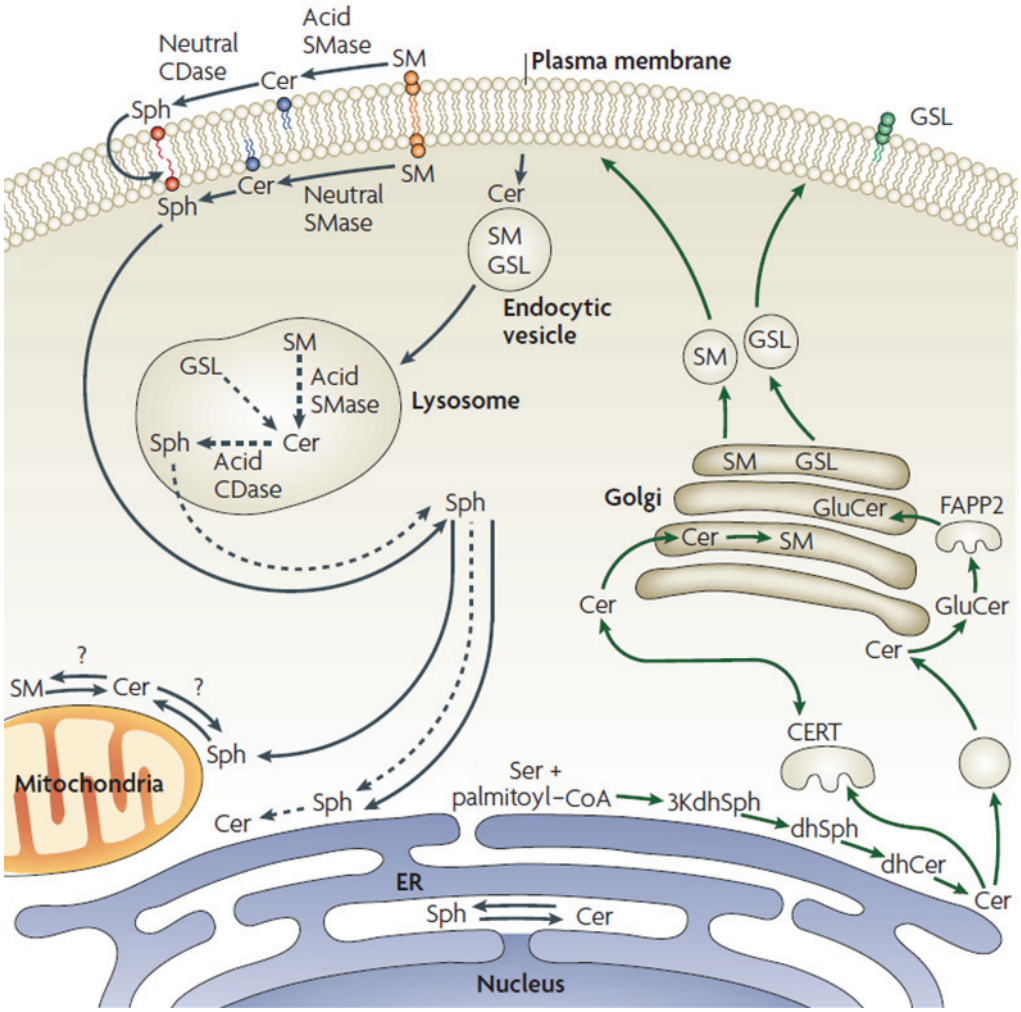

Fig. 1.2. Sphingolipid metabolism. *De novo* synthetic pathway of sphingolipids is depicted by green arrows. *De novo* synthesis of ceramide (**Cer**) occurs in the cytosolic side of the endoplasmic reticulum (**ER**) and possibly in ER-associated membranes, such as the perinuclear membrane. The newly synthesised Cer is transported to the Golgi by either vesicular or non-vesicular transport. The non-vesicular transport of Cer is mediated by ceramide transfer protein CERT which specifically delivers Cer for the synthesis of sphingomyelin (**SM**) [15]. The Cer transported by vesicles enters glycosphingolipid (**GSL**) synthesis pathway. Glucosylceramide (**GluCer**) is synthesised on the cytosolic side of the Golgi membrane and transferred to distal Golgi compartments. This can be accomplished by the flow of Golgi membrane – vesicular transport/cisternal maturation [17] (not shown), or by non-vesicular transport mediated by protein FAPP2 [18]. Further synthesis of GSLs takes place in the lumen of the distal Golgi compartments. Thus GluCer is translocated from cytosolic to luminal leaflet of the Golgi membrane [14]. Delivery of Golgi-synthesised SM and complex GSLs to the plasma membrane occurs by vesicular transport. Acid sphingomyelinase (**SMase**) present in the outer leaflet of the plasma membrane or neutral SMase in the inner leaflet can metabolize SM to Cer, and thus new Cer may also be generated on the plasma membrane. SM and GSLs can be internalised through endosomal pathways and reach a lysosomal compartment, where they are degraded by SMase and glucosidases to form Cer [14]. Finally, Cer is hydrolysed by acid ceramidase (**CDase**) to form sphingosine (**Sph**). It is postulated, that Sph may be salvaged from lysosomal degradation and recycled back to ER for synthesis of Cer [14]. Salvage pathway is depicted in dashed arrows. The figure is modified from a review article by Hannun and Obeid [14].

1.1.3. Functions of glycosphingolipids

Since the discovery of the most common GSLs such as GluCer, GalCer, sulfatide, LacCer and brain gangliosides in 1960s [19], extensive effort has been made to understand their role (in the context of a single cell and that of a whole organism). GSLs were found to interact with specific functional proteins such as integrins, growth factor receptors and be important for the localisation of signal transducers (e.g. Src family kinases [20]). Moreover, GSLs were shown to be involved in cell adhesion, signal transduction, phenotype determination, growth, motility and differentiation [19]. Some examples on how these processes depend on GSLs are mentioned below.

A concept of "glycosynapse", a membrane microdomain involved in carbohydrate-dependent cell adhesion and signal transduction events, was introduced by Hakomori in 2002, emphasising the role of GSLs in signalling across the cellular membrane [21]. The concept is based on numerous examples of positive and negative effects on signal transduction which are described for specific GSLs, e.g. (i) ganglioside GM3 interacts with the extracellular part of the epidermal growth factor receptor (EGF-R) and inhibits tyrosine phosphorylation without affecting binding of the ligand [22], (ii) binding of Shiga toxin to its receptor, globotriaosylceramide (Gb3), activates Syk kinase and induces signalling which facilitates endocytosis of the toxin [23].

The expression of certain GSLs is strictly regulated during embryonic development suggesting their implication in the determination of the cell fate [21;24]. *In vivo* studies on genetically engineered mice with disrupted genes for specific glycosyl-transferases revealed that GluCer, the precursor for majority of complex GSLs, was essential for embryonic development and cellular differentiation. Offspring lacking active glucosylceramide synthase showed embryonic lethality at a very early stage [25;26]. The knock-out of individual glycosyl-transferases, involved in synthesis of more complex GSLs, displayed less profound or no effects in mouse models suggesting functional subdivision among complex GSLs: the functional role of the missing GSL may be taken over by existing GSLs and therefore no well-defined changes can be observed [26].

Multiple GSLs are recognised as tumour-associated antigens [21]. Cancer related changes in glycosylation are described in 1.2.

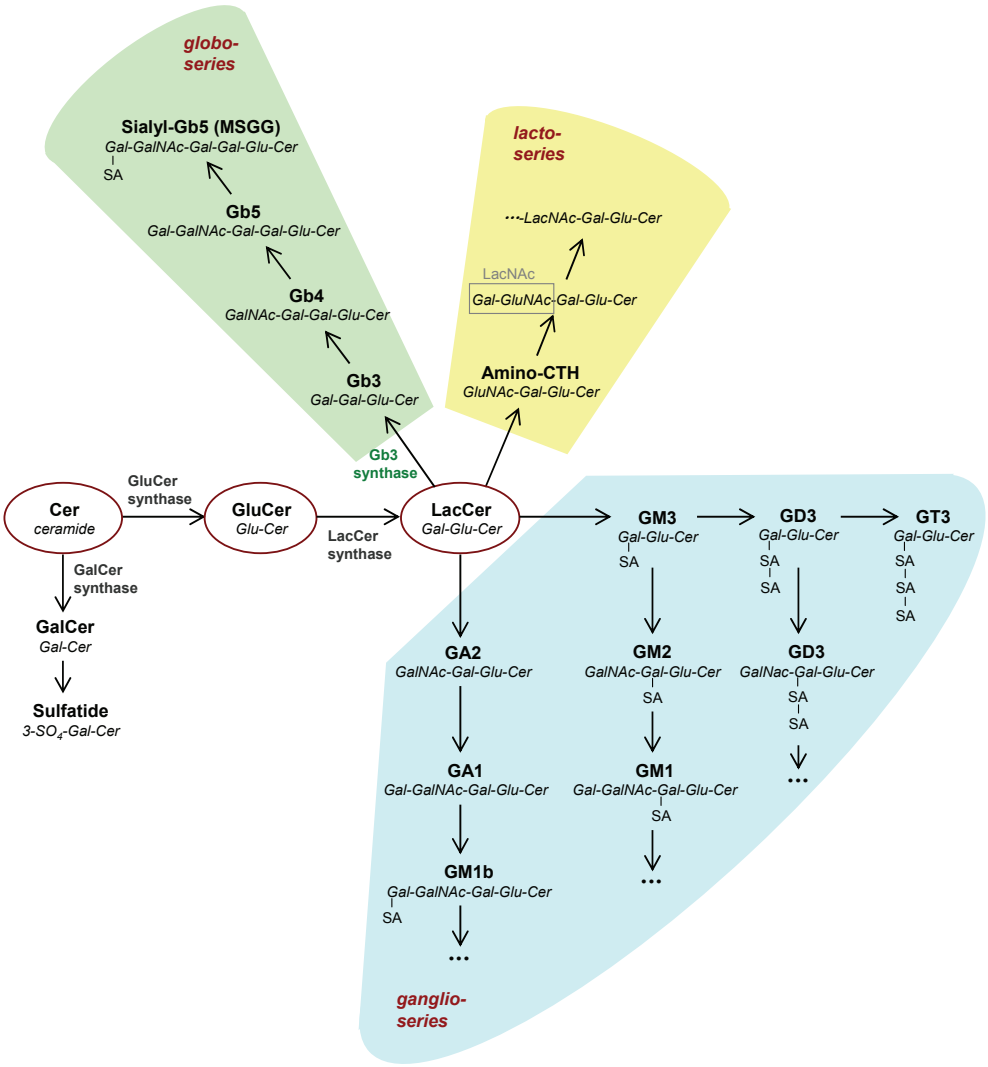

Fig. 1.3. Synthesis of glycosphingolipids. Glucosylceramide (**GluCer**) is used as a precursor for the synthesis of majority of GSLs in the cell, while galactosylceramide (**GalCer**) is metabolised only to a few GSLs, such as sulfatide [27]. Based on the core structure of the carbohydrate chain, lactosylceramide (**LacCer**)-originated GSLs are subdivided into three subclasses: globo-, lacto- and ganglio-series GSLs [19]. **GalNAc** – N-acetylgalactosamine, **GluNAc** – N-acetylglucosamine, **SA** – sialic acid, **Amino-CTH** – glucosaminyl lactosyl ceramide. The figure is modified from Furukawa *et al.* [27].

1.1.4. Globotriaosylceramide (Gb3)

Globotriaosylceramide (Gal-α1→4Gal-β1→4Glu-β1→Cer, Gb3) is the first product in the synthetic pathway of globo-series GSLs (Fig. 1.3). Gb3 is synthesized from LacCer by the addition of one galactose, and the reaction is catalysed by Gb3 synthase (α-1,4-galactosyltransferase) [1] (Fig. 1.4).

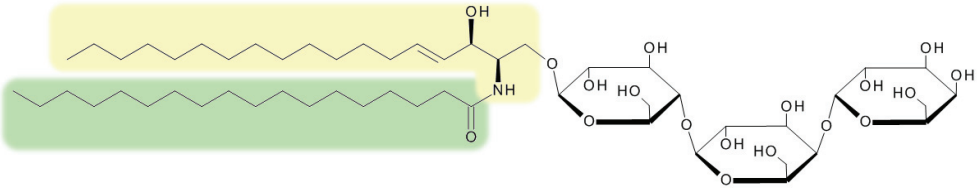

Fig. 1.4. Chemical structure of globotriaosylceramide (Gb3). The sphingosine (highlighted in yellow) most often contains chain length of 18 carbon atoms, whereas the fatty acyl chain (highlighted in green) varies both in length and saturation (here shown as C18:0). The sugar chain is: Gal-α1→4Gal-β1→4Glu-β1→(Cer). The bond α1→4Gal at the core of the sugar chain is a distinct characteristic to all globo-series GSLs.

The expression of Gb3 is not homogenous throughout the human body. Normally, the highest levels of Gb3 are found in the kidney epithelium and endothelium [2-4], in microvascular endothelial cells [5;6] and in platelets [7]. In carbohydrate defined P histo-blood group system, Gb3 constitutes the rare P^k antigen present on the erythrocytes [28]. In the immune system, Gb3 represents a lymphocyte differentiation antigen, termed CD77, which is expressed in a subset of germinal centre B lymphocytes [29]. However, it is still unclear why Gb3 is highly expressed in certain types of tissues and is absent in others.

Elevated levels of Gb3 have been demonstrated for several conditions including Fabry disease [30;31] and a number of cancer types such as metastatic colon cancer [8;9;32] and B cell lymphomas [33-36]. However, the physiological role of Gb3 is still unclear. *In vivo* studies on Gb3 synthase knock-out mice, which displayed a total loss of Gb3 and other globo-series GSLs, showed no changes in birth-rates and no apparent abnormalities over a year of nurturing, with the exception of total loss of sensitivity to Shiga-like toxins as compared to wild-type mice [37].

Binding of different ligands to Gb3 may trigger different signalling pathways in the cells. It has been shown that anti-Gb3/CD77 mAb and Shiga-like toxin 1 (see below) induce apoptosis in Burkitt's lymphoma cells by different mechanisms: Shiga-like toxin 1 triggers a caspase and mitochondria-dependent apoptotic pathway, while binding of anti-Gb3/CD77 mAb induces caspase-independent and oxidative stress-dependent signalling for apoptosis [38]. This indicates that Gb3 may be involved in several cellular events and a more comprehensive understanding of its functions is needed.

Gb3 serves as a receptor for plant and bacterial protein toxins, such as ricin, Shiga toxin and Shiga-like toxins. Naturally, toxins cause damage to cells and thus lead to occurrence of a

disease; however, they can also be employed for research and diagnosis/therapy in the medicine [1;39]. The toxins, used in this study, are discussed in 1.3.

1.1.5. 2-deoxy-D-glucose and sodium butyrate as modulators of Gb3 biosynthesis

Two compounds, 2-deoxy-D-glucose (2DG) and sodium butyrate, reported to affect Gb3 synthesis, were employed in this study.

2DG is a structural analogue of glucose, differing from glucose only by the absence of one oxygen atom at the second carbon. Although structurally very similar to glucose, 2DG is not metabolized by cells, and it induces multiple responses. The most apparent effect of 2DG is the inhibition of glycolysis by competitive inhibition of glucose transport and phosphorylation by hexokinase [40;41]. 2DG has been also shown to interfere with cell cycle control [42] and DNA repair [43], and not necessarily by the mechanisms dependent on glycolysis inhibition [44]. Of particular interest to this study, was a recently observed inhibitory effect of 2DG on the expression of the Gb3 synthase and a resulting reduction of cellular Gb3 [45]. Although 2DG has been previously demonstrated to have a repressive effect on gene expression, which is mediated indirectly by inhibition of glycolysis [46], activation of the class III histone deacetylase SIRT1 [47] or enhanced *O*-GlcNAc modification of transcriptional factor Sp1 [48], non of these mechanism were found to be involved in the inhibition of Gb3 synthase [45].

Sodium butyrate is a sodium salt of butyric acid which is a short chain fatty acid secreted as a by-product of polysaccharide metabolism by the colonic bacterial flora [49]. Butyrate is demonstrated to induce differentiation and suppress proliferation of various human malignant [50;51] and normal cells [52] *in vitro*. Butyrate regulates gene expression (may act as a stimulator or as a repressor) through the inhibition of histone deacetylases which are involved in chromatin remodelling [53], and therefore induces multiple responses in the cells. Of particular interest to this study, is the ability of butyrate to sensitize cells to Shiga toxin and ricin, and even to induce changes in the composition of fatty acids in the ceramide part of the Shiga toxin receptor glycosphingolipid Gb3 [54].

1.2. Cancer

Cancer is a class of diseases characterized by abnormal cell growth and invasion to surrounding tissues and/or distal organs. The incidence of most cancers was growing during the past years, and it was estimated to be a cause of death for more than 1.5 million people in Europe in 2008 [55]. High cancer mortality is mainly related to metastases, which are challenging to diagnose and treat.

1.2.1. Metastasis

Metastasis is a multistage process by which malignant cells leave the primary tumour and spread to distant organs [56]. There are several critical steps that have to be accomplished by metastasizing cancer cells (Fig. 1.5). During cancer progression cells undergo numerous genetic and biochemical changes which lead to changed morphology and behaviour, enabling them to invade distant organs. The ability to migrate and invade is one of the crucial changes for the occurrence of metastasis, which enable cancer cells to leave the primary tumour, enter blood or lymph circulation, and finally re-enter a new location [57].

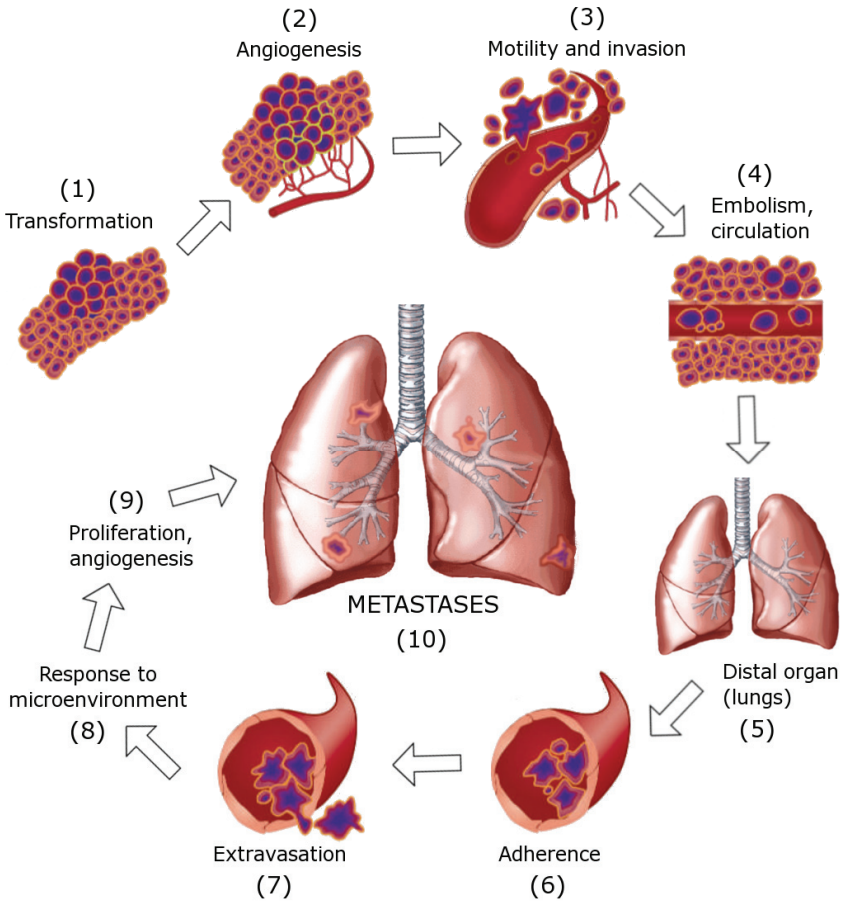

Fig. 1.5. Development of metastases. (1) Cellular transformation and tumour growth; (2) Tumour vascularisation; (3) Local invasion of the host stroma (the most common route is through lymphatic channels); (4) Detachment and circulation of single or aggregated cancer cells in blood and lymph; (5) Survived cancer cells reach distal organs; (6) Adherence to capillary endothelial cells; (7) Extravasation into organ parenchyma; (8-10) Proliferation of tumour cells and angiogenesis, resulting in metastasis. The process can be reinitiated and secondary metastases may develop from the initial metastasis. The figure is modified from a review article by Talmadge and Fidler [56].

1.2.2. Cancer cell migration

Different types of cancer cell migration have been observed during metastasis, and are classified into single- or collective- cell migration. Furthermore, it has been suggested that cells of different origin may favour a particular type of migration, e.g. colon cancer cells often migrate as a single cell, while squamous cell carcinomas invade predominantly in a collective type of cell migration [57]. Due to the questions studied in the present work, only single-cell migration is discussed here.

Based on morphology, single-cell migration is subclassified into a mesenchymal and an amoeboid migration, and both mechanisms can be exploited by metastasing cancer cells. The

mesenchymal cell migration is driven by a leading edge with membrane protrusions and actin polymerization such as stress fibers, and firm integrin-mediated adhesion to the matrix. On the contrary, cells which migrate by an amoeboid manner are round in their shape and form neither mature focal adhesions, nor stress fibers [58]. Moreover, in order to pass the barrier of the extracellular matrix, the mesenchymally migrating cells depend on metalloproteases which cleave the collagen fibers (the main component of the stromal extracellular matrix). Alternatively, cells migrating by the amoeboid manner are shown to be able to squeeze through collagen-lined pores without proteolytic degradation of the matrix. However, it is still unclear if metalloprotease-independent cell migration plays a significant role in cancer cell migration [59].

In order to leave a solid primary tumour and invade surrounding tissue, cancer cells are thought to undergo multiple inter- and intracellular changes by a process termed epithelial-to-mesenchymal transition (EMT) [57;60]. A central hallmark of EMT is a process, termed cadherin switch, a loss of the epithelial cell-cell adhesion molecule E-cadherin, and concomitant expression of the mesenchymal cell-cell adhesion molecule N-cadherin. The cadherin switch leads to cell separation from its "neighbours" [61]. Furthermore, the N-cadherin is suggested to influence tumour cell behaviour via the interaction with the receptor tyrosine kinases. For example, N-cadherin has been shown to interact with fibroblast growth factor receptor and prevent its internalization, resulting in increased levels of the receptor on the surface and enhanced downstream signalling [62].

Other pivotal cellular players in the cell migration are members of the Rho GTPase family, which transduce signal from growth factor and cell adhesion receptors to effector proteins responsible for actin cytoskeleton remodelling. For instance, GTPases Rac1 and Cdc42 induce plasma membrane protrusions, such as lamellipodia and filopodia, while RhoA regulates cell-cell and cell-matrix adhesion, and is involved in the tail detachment at the back of the migrating cell [63].

The majority of cell adhesion and recognition events are considered to be mediated by protein-protein interactions, which can be homotypic (between proteins of the same kind, e.g. between cadherin receptors [64]), or heterotypic (between different proteins, e.g. between integrins and extracellular matrix proteins [65]). In addition, two other types of interactions involved in cell adhesion and recognition processes are described: (i)

interactions based on glycosyl epitopes of glycoproteins or GSLs recognition by carbohydrate binding proteins, i.e. lectins, and (ii) direct interactions between carbohydrate chains of GSLs [19]. Therefore, GSLs may also play a crucial role in cancer cell migration.

1.2.3. Glycosylation and cancer

Changes in the glycosylation pattern are observed in all human cancer types and very often relate to their invasiveness and metastasis: high expression of some glycosyl epitopes correlates with shorter patient survival rates, while other glycosyl epitopes suppress tumour progression and lead to higher survival rates following anti-cancer treatment [66]. Aberrant glycosylation may occur both in glycoproteins and glycolipids; however, this chapter is focused on aberrant glycosylation in GSLs. Further on, several GSLs are discussed in relation to cancer.

Cancer related alterations in GSLs may occur in carbohydrate structure [67] and/or the composition of the ceramide [68]. They can also manifest themselves as up- or down-regulation of certain GSLs. Several GSLs are characterized as human tumour-associated antigens. For example, Gb3 has been found to be characteristic for several types of B cell lymphomas [33-36], colon carcinoma [8;9;32], breast cancer [36], testicular cancer [69] and acute non-lymphatic leukaemia [70], while over-expression of GD3 is characteristic to human melanomas [71;72]. On the other hand, ganglioside GM3 has been found to be down-regulated in metastatic forms of bladder tumours [73]. Moreover, a correlation between virus-induced oncogenic transformation and lowered levels of GM3 has been demonstrated in several cell cultures [74;75]. However, the anti-cancer role of GM3 is not clear yet, because opposite effects on GM3 levels were also observed [76]. Seemingly, the ratio between different GSLs might be a more important determinant in the disease progression than up- or down- regulation of only a single GSL.

1.2.4. Colon cancer

Colon cancer was estimated to be the most common type of cancer in Europe in 2008, and with the death rate close to 50%, colon cancer was also expected to be one of the most common cause of death from cancer [55]. While benign tumours can be surgically removed,

the treatment of malignancies is much more complicated. Metastases spread to distant organs are challenging to detect and treat, and therefore there is a huge demand for novel diagnostic and therapeutic techniques for effective treatment of metastatic colon cancer.

Gb3 was recently demonstrated to be a potential target for treatment of colon cancer. The expression of Gb3 was shown to be elevated in human tissue samples from primary metastatic colonic tumours and their liver metastasis in contrast to benign tumours. This suggested that Gb3-expressing colon cancer cells represented a potentially invasive sub-population [8]. Moreover, upregulation of Gb3 synthase in benign colon cancer cells was sufficient to drive their transition to the invasive form [8], suggesting that Gb3 may play an important role in colon cancer progression. Further investigation might reveal novel strategies for the effective treatment of colon cancer.

1.2.5. Colon cancer cell lines used in this study

Two colon cancer cells lines, SW480 and HT-29, were used as *in vitro* model systems in this study and are featured in the following paragraphs.

The SW480 cell line was isolated from the primary adenocarcinoma arising in the colon [77]. Later, this cell line was found to consist of two distinct sub-populations, which were designated as E-type (epithelial) and R-type (round) [78]. The E-type cells form flat epithelial-like colonies and constitute a majority (> 98%) of SW480 cells, while only a small fraction (< 2%) is round in the shape and grows in clusters of piled-up cells. Both sub-populations were shown to be stable when cultured separately, and exhibited multiple differences from each other both *in vitro* and *in vivo*. The R-type sub-population had half the doubling time of the E-type, poor plate adhesiveness, and produced twice as big and less differentiated tumours when injected to mice compared to the E-type cells. Both sub-populations were shown to have similar point mutations, and therefore were suggested to be of the same origin [78]. Later, other groups compared metastatic potentials of these two sub-populations, and demonstrated that the E-type had a higher colony forming efficiency, higher motility and invasion *in vitro*, and was capable of forming metastasis *in vivo*, in contrast to the R-type cells. However, tumours derived from E-type cells had a high frequency of spontaneous regression, which was not observed for tumours formed by the

cells of R-type. Therefore, there was no clear conclusion as to which subpopulation represented a more aggressive form of cancer [79].

The SW480 cell line was chosen for this study, because it was shown to migrate spontaneously *in vitro* [80], and it diversely expresses glycosphingolipid Gb3, which made it a potential model for studying the impact of Gb3 on cell motility.

The HT-29 cell line is a human colorectal adenocarcinoma cell line isolated from a moderately differentiated primary tumour [51;81]. The HT-29 cells closely resemble small intestinal crypt cells and even have a capacity to differentiate into a more villus-like phenotype *in vitro*, e.g. in response to sodium butyrate treatment [50]. Since HT-29 cells resemble a more differentiated form of colon cancer than SW480 cells, the HT-29 cell line was chosen for this study to investigate the differences between various cell lines and their responsiveness to treatment.

1.3. Protein toxins

Protein toxins are produced by certain bacteria and plants, and function as autonomous killing devices, which target specific cells and modify specific intracellular components. Protein toxins vary in their structure, receptor (and therefore cell type), their intracellular target and the mechanism of intoxication. In this study, four different protein toxins, Shiga toxin, Shiga like toxin 2, diphtheria toxin and ricin, were employed, and therefore are discussed in following paragraphs. The last part of the chapter is dedicated to a short review on protein toxin applications in research and medicine.

1.3.1. Shiga toxins

Shiga toxins comprise a family of related protein toxins, which are similar in their structure (Fig. 1.6) and the mechanism of action, but are produced by different types of bacteria. Shiga toxin (Stx) is secreted by *Shigella dysenteriae*, whereas Shiga-like toxins are produced by certain strains of *Escherichia coli* and some other bacteria. Shiga-like toxin 1 (SLT-1) differs from Stx only in one amino acid residue in the catalytic A-moiety of the toxin, whereas Shiga-like toxin 2 (SLT-2) shares only ~60% sequence similarity with Stx and is immunologically distinct [1].

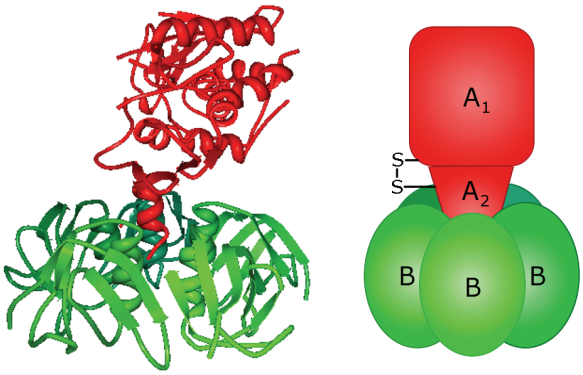

Fig. 1.6. The structural and schematic models of Shiga toxin. Shiga toxins consist of two non-covalently linked moieties: an A-moiety of ~32 kDa, and a B-moiety, comprised of five 7.7 kDa B-chains. During intracellular toxin transport, the A-moiety is cleaved by the protease furin into two fragments: an enzymatically active A_1 fragment (~27 kDa), and a carboxyl terminal A_2 fragment, which remains linked by a disulfide bond until arrival to the ER [1;39]. The structure image was prepared using PDB ProteinWorkshop 3.9 (PDB protein data bank: 1DM0).

Shiga toxins bind to the cell surface through the interaction between the B-moiety and Gb3. All Shiga family toxins, except for one SLT-2 variant, SLT-2e, which can bind to Gb4, possess a high specificity for Gb3 [82]. The homopentameric B-moiety has multiple binding sites (three potential trisaccharide-binding sites per B fragment [83]) for Gb3, and therefore can achieve a high binding affinity for cells. Although in theory, one Stx molecule can simultaneously bind up to 15 Gb3s, not all binding sites have equal affinity for the carbohydrates of Gb3, and, therefore, not all sites might be required for binding to the cell surface, but rather mediate additional recognition and membrane remodelling [84;85]. Furthermore, the lipid composition of the plasma membrane (particularly the level of cholesterol) and types of fatty acids in the ceramide moiety of Gb3 are demonstrated to modulate the interaction between Shiga toxins and the receptor [86;87]. However, SLT-2 differs in binding from Stx and SLT-1. Although SLT-2 is demonstrated to have lower affinity for Gb3 than SLT-1 [88], it is much more lethal in animal models [89;90] and is thought to be the main cause of life threatening infections in humans [91]. The gastrointestinal infection with SLTs producing *E. coli* serotypes is highly dangerous to children and adolescents, as it may lead to a severe complication, haemolytic uremic syndrome (HUS), which involves kidney damage [92].

The B-moiety alone is not toxic to cells (with exception of B cells, where it may induce apoptosis [93]) and functions as a delivery tool for the enzymatically active A-moiety. Upon internalization, which may occur through clathrin-dependent and clathrin-independent

endocytic pathways [39], the A-moiety is cleaved by the protease furin in two fragments, A_1 and A_2 (Fig. 1.6), which remain linked to each other by the disulfide bridge. For the cytotoxic action, the toxin needs to be transported retrogradely to the Golgi, and further to the endoplasmic reticulum (ER) [94], where the internal disulfide bond is reduced and the enzymatically active A_1-fragment is translocated and released into the cytosol [39]. The A_1-fragment then inhibits protein synthesis by cleaving one adenine residue from the 28S RNA of the 60S ribosomal subunit [95]. Moreover, the action of Shiga toxins in the cells is not limited to the inhibition of protein synthesis, and other cellular responses such as cytokine expression and apoptosis have been shown to be triggered by the toxin [82].

1.3.2. Diphtheria toxin

Diphtheria toxin (DT) is secreted by *Corynebacterium diphtheriae* as a single-chain polypeptide with a molecular weight of ~58 kDa. DT belongs to the A-B family of toxins and it consists of two moieties: an enzymatically active A-moiety (~21 kDa), and a B-moiety (~37 kDa), which has a transmembrane T-domain and a receptor binding R-domain (Fig. 1.7) [96]. In the first step of the intoxication process, DT binds, via its R-domain, to the heparin-binding epidermal growth factor precursor (pro-HB-EGF) [97] and undergoes receptor-mediated endocytosis in a dynamin-dependent manner [98]. Upon binding to the receptor, DT is cleaved by the protease furin in two fragments: the A- and B-moieties, which stay linked to each other by the disulfide bridge [99]. The low endosomal pH then triggers the conformational changes and the insertion of the T-domain into the endosomal membrane, and aid the translocation of the A-moiety from the endosomes to the cytosol [100-102]. At some point, probably during exposure to the cytosol, the reduction of the disulfide bond between A- and B-moieties occurs, and the enzymatically active A-moiety is released to the cytosol [96;100;103]. The A-moiety catalyzes ADP-ribosylation of the elongation factor 2, resulting in the inhibition of protein synthesis [104;105].

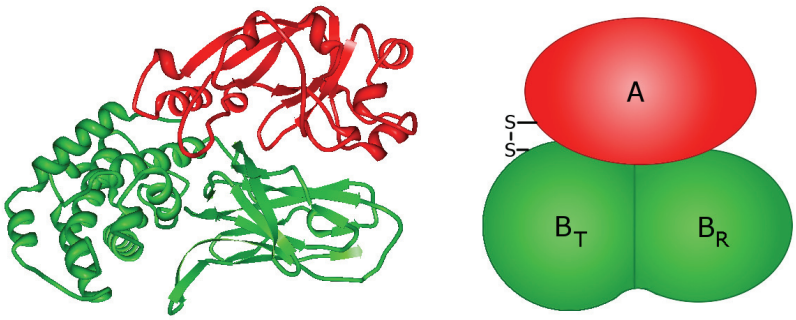

Fig. 1.7. The structural and schematic models of Diphtheria toxin. Diphtheria toxin consists of two moieties: an enzymatically active A-moiety (~21 kDa) and a B-moiety (~37 kDa), which has a transmembrane T-domain and a receptor binding R-domain. During intoxication, the host protease furin cleaves the peptide bond between the A-moiety and the T-domain, but the A- and B-moieties remains linked by a disulfide bond [99]. The structure image was prepared using PDB ProteinWorkshop 3.9 (PDB protein data bank: 1F0L).

1.3.3. Ricin

Ricin is a toxic carbohydrate-binding protein, which is present in the seeds of the castor bean plant (*Ricinus communis*). Ricin belongs to the same A-B family of toxins, as diphtheria toxin, and consists of two functionally different parts: an enzymatically active A-moiety (~30 kDa) and a receptor binding B-moiety (~30 kDa) [106]. The two moieties are represented by two individual polypeptide chains, which are linked to each other by a disulfide bridge (Fig. 1.8) [107]. Ricin does not have a single receptor, and binds, via its B-moiety, to both glycoproteins and glycolipids with terminal galactose, ant therefore is not selective to a given cell type [108]. Furthermore, a depletion of GSLs does not protect cells against intoxication with ricin, confirming that ricin exploits multiple targets on the cells [109;110]. Upon binding, ricin is taken up by different endocytic mechanisms, i.e. its uptake does not depend on a certain endocytic pathway. For example, ricin is still efficiently taken up by cells after inhibition of both clathrin- and caveolae-dependent endocytic mechanisms (the cells were stably expressing mutant dynamin, end were depleted from cholesterol) [111].

The intoxication with ricin is similar to Shiga toxins by requiring retrograde sorting to the Golgi, and further to the ER, where the enzymatically active A-moiety is translocated and released to the cytosol [112;113]. The A-moiety possesses N-glycosidase activity and catalyses cleavage of one adenine residue from the 28S RNA of the 60S ribosomal subunit, leading to the inhibition of protein synthesis [114].

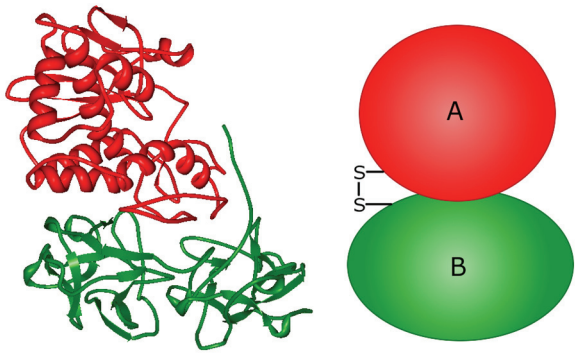

Fig. 1.8. The structural and schematic models of ricin. Ricin consists of two moieties: an enzymatically active A-moiety, and a binding B-moiety. Both moieties are of similar size (~30 kDa), and are linked together by a disulfide bridge [106;107]. The structure image was prepared using PDB ProteinWorkshop 3.9 (PDB protein data bank: 2AAI).

1.3.4. Toxins as tools

Toxins have been found to be valuable tools in research and medicine, and several such examples are described bellow.

Toxins are employed to study endocytosis, intracellular transport and signalling pathways. For instance, several ADP-ribosylating toxins target specific GTP-binding proteins. DT targets elongation factor 2 and thus inhibits protein synthesis, whereas cholera toxin targets the α-subunit of heterotrimeric G_s protein, and renders its persistent activity, leading to several cellular responses such as increased cyclic AMP levels and protein phosphorylation [115]. Furthermore, studies on transport mechanisms employed by toxins, such as Stx and ricin, help to reveal endocytic and intracellular trafficking processes [39].

Protein toxins can be used by several means in medicine: (i) as carriers, which transfer a coupled molecule to specific cells/tissues, (ii) as diagnostic tools, when coupled to an imaging molecule, or (iii) as highly efficient drugs, which are modified to be specifically targeted. The latter approach is based on toxin conjugation with, e.g. an antibody or a growth factor, which provides specific targeting of the toxin. The first clinically approved toxin derivative (denileukin diftitox) is a recombinant fusion protein of diphtheria toxin (without receptor binding domain) and human interleukin 2, and is used for the treatment of cutaneous T cell lymphoma [116]. Multiple other toxin derivatives are now being investigated for the treatment of various conditions, including cancer, AIDS and allergy [117-119].

Biochemically engineered toxins can also be employed for the diagnosis of cancer. The non-toxic binding moiety of the toxin can be labelled with an imaging molecule, such as fluorophore (for the optical/fluorescence detection), with positron emitters, such as ^{18}F and ^{11}C, for detection by positron emission tomography (PET), or gamma emitters, such as ^{99m}Tc, for single photon emission computed tomography (SPECT) [1]. For instance, fluorescently labelled B-moiety of Stx has been demonstrated to target specifically human colorectal carcinomas in mice models [120].

2. Materials and Methods

2.1. Materials

2.1.1. Reagents and solutions

A detailed list of reagents and solutions used in this study is given in the Appendix.

2.1.2. Antibodies and primers

Antibodies

Isotype	Against	Species, raised in	Conjugated to	Producer	Cat. No.
IgM	Gb3 (CD77), human	Mouse	-	BD Pharmingen	551352
IgG	Shiga toxin	Mouse	-	Toxin Technology	13C4
IgM	Mouse	Goat	Rhodamine red X	Jackson	115295075

Primers for qRT-PCR

Name	Producer	Product No.
QuantiTect Primer Assay for Gb3 synthase	QIAGEN	QT00204652
TBP forward 5′-GCCCGAAACGCCGAATAT-3′	MWG-Biotech AG	Custom-made
TBP reverse 5′-CGTGGCTCTCTTATCCTCATGA-3′	MWG-Biotech AG	Custom-made

2.1.3. Toxins

Stx was a gift from J.E. Brown (USAMRIID, Fort Detrick, MD, USA). SLT-2 was a gift from J. Müthing (Institute for Hygiene, Food Chemistry, Germany). DT was purchased from Connaught Laboratories (Canada, Toronto), and ricin was purchased from Sigma-Aldrich.

The plasmid expressing StxB-sulf2 was a gift from Dr. B. Goud (Institute Curie, Paris, France), and StxB-sulf2 was prepared as described by Lauvrak *et al.* [23].

2.1.4. Cell lines

All cells used in this study were subcultured twice a week by assisting personnel of the department. HEp-2 and SW480 cell lines were purchased from The American Type Culture Collection (ATCC). HT-29 cell line was provided by M. Eknes (Department of Cancer Prevention, Institute for Cancer Research, Oslo). Short characterization of each cell line is given below.

HEp-2

The HEp-2 cell line was established by Dr. Audrey Fjelcte in 1952. It was originally thought to be epidermoid carcinoma, obtained from a man with a primary tumour of the larynx [121], but later it was discovered to be derived via HeLa contamination [122].

HEp-2 cells were cultured in complete DMEM growth medium at 37 ^{o}C in a 5% CO_2 atmosphere.

SW480

The SW480 cell line was established in Scott and White Clinic (Texas) in 1975. It was isolated from primary adenocarcinoma of the colon [123]. The SW480 cell line consists of two distinct subpopulations, designated as E-type (epithelial) and R-type (round) [78]. These two subpopulations display different tumorigenic, invasive and metastatic potential [79].

SW480 cells were cultured in complete RPMI 1640 growth medium at 37 ^{o}C in a 5% CO_2 atmosphere.

HT-29

The HT-29 cell line is a human colorectal adenocarcinoma cell line isolated from a Caucasian woman in 1964 [124]. Morphologically, these cells are round-shaped with microvillus-like structures, and they form compact colonies when growing in dense cultures.

HT-29 cells were cultured in complete DMEM/F12 growth medium at 37 ^{o}C in a 5% CO_2 atmosphere.

2.1.5. Instruments

Liquid Scintillation Counter 2100TR (Packard)

The liquid scintillation analyzer detects small amounts of radioactivity, and was used for assaying the inhibition of protein synthesis in this study. The principle underlying liquid scintillation counting is that radioactive emission from the sample is converted to a visible light, which then is detected by a photomultiplier tube in the instrument [125]. The conversion from radioactive to electromagnetic energy is fulfilled when a scintillating molecule (usually fluor) is exited by radioactive emission and releases the energy as an electromagnetic wave (UV light in the case of fluor). The instrument counts burst of light – fluorescence of fluor – and records it as counts per minute (cpm), which are proportional to the amount of radioactive molecules in the sample. In the protein synthesis assay, cpm value is proportional to [^{3}H]leucine incorporated into the proteins during their synthesis, and it was used to quantify protein synthesis activity in the cells.

Microplate reader: M1R Analyzer (BioVeris)

The M1R Analyzer is a multi-well microplate-based instrument for electrochemilumine-scence detection, which was used in the endocytosis of biotin-Shiga toxin assay. Upon activation by electric current, an electrochemiluminescent compound – ruthenium (II) trisbipyridine (commercially named BV-TAG) – emits a photon of 620 nm (red light) and returns to its initial state. The activation/emission cycle can be repeated many times, which leads to an amplification of the signal [126]. BV-TAG can be chemically linked to various molecules and thereby make these molecules detectable by the M1R Analyzer.

In order to be excited, BV-TAG needs to be attached to the electrode in the instrument. This is fulfilled by the attraction of paramagnetic beads to the magnet (step 2 in the Fig. 2.1). Paramagnetic beads are used as carrier molecules and need to be linked to a target molecule during the experimental procedure. During the detection, the magnet is removed and an electric current is applied to the electrode. This causes the excitation of BV-TAG and detection of red light by the instrument (step 3 in the Fig. 2.1).

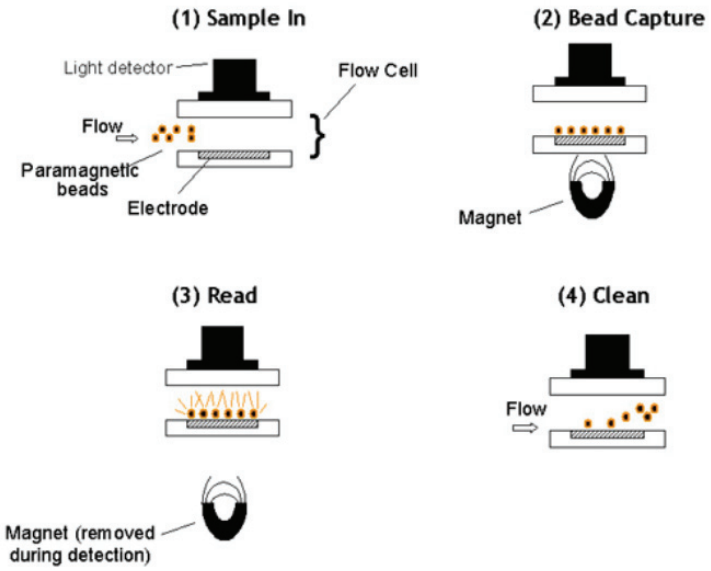

Fig. 2.1. Detection by M1R Analyzer. Picture is taken from M-SERIES® M1R Analyzer User Guide [126].

2.2. Methods

2.2.1. Toxicity Assays

Cell counting

Cells were cultured in 6- or 24-well culture plates with or without (control) a particular drug. The medium was removed, cells were washed with a small volume of trypsin/EDTA solution (37 ^{o}C), 0.5 ml (for 24-well plate) or 1.0 ml (for 6-well plate) trypsin/EDTA solution (37 ^{o}C) was added to each well, and plates were placed back in a 5% CO_2 incubator for 8 min. Cells were mixed by pipetting up and down several times and inspected using a microscope with phase contrast to see if they were detached. If some of the cells were still attached to the bottom of the well, the plate was placed back into the incubator for additional 2 min. Finally, 0.5 ml (for 24-well plate) or 1.0 ml (for 6 well plate) HEPES medium was added to each well, and 400 µl cell suspension was then transferred to counting tubes containing 20 ml ISOTON II diluent. Cells were counted by a Particle Counter Z1 (Beckman Coulter). A tube containing fresh ISOTON II diluent was counted between each sample to wash the system of previously counted cells.

Protein content measurement

Cells were cultured in 6- or 24-well culture plates with or without (control) a particular drug. After incubation, the medium was removed from all wells; the plates were placed on ice, and all wells were washed with cold (+4 ^{o}C) PBS. Then, 200 µl (for 24-well plate) or 400 µl (for 6-well plate) freshly prepared cell lysis solution was added to all wells, and the plates were kept on ice for 10 min. Cells were scraped (using 1 ml pipette tip), pipetted up and down, and transferred to clean 1.5 ml Eppendorf tubes. Lysates were centrifuged at 5200 x g for 10 min at 4 ^{o}C to remove nuclei. Duplicates of 25 µl of supernatant were transferred to a 96-well plate (10 µl of total cell lysates were used when performing the biotin-Shiga toxin endocytosis assay). Pierce® BCA protein Assay Kit was used for total protein detection in these samples. Bovine serum albumin (BSA) dilutions in the cell lysis solution in the range of 25-2000 µg/ml were used to make a standard curve when measuring protein content for the first time (dilutions prepared according to instructions given in the protocol for Pierce®

BCA protein Assay Kit, Nr. 23225, Thermo Scientific). This curve was used to estimate if the protein amounts in the samples corresponded to the linear range of the calibration curve. When the experiment was repeated with similar conditions, a calibration curve was not used and the protein amount in the samples was estimated relative to the control group. Freshly prepared working reagent (mixture of kit reagents A and B by ratio 1:50) was added to the wells containing samples, BSA dilutions or cell lysis solution (blank). The plate was covered with Parafilm, briefly shaken and incubated at 37 ^{o}C for 30 min. Then the plate was taken off the incubator and allowed to cool down to room temperature (RT) for 30 min. Finally, absorbance at 562 nm was measured with a Synergy 2 (BioTek) plate reader. The absorbance of blank wells was subtracted from absorbance values measured for the sample wells prior to relative quantification. The relative protein amount (RPA) for treated samples was calculated according to the equation: RPA = A_{562}(*sample*)/A_{562}(*control*).

2.2.2. Protein Synthesis Inhibition Assay

Cells were seeded in 24-well culture plates one day prior to the experiment. Seeding densities were 5 x 10^4 cells/well for short incubation experiments and 3 x 10^4 cells/well for long incubation (1-2 days) experiments. Next day, treatment with the drug (or combination of drugs) started and cells were incubated at 37 ^{o}C in a 5% CO_2 atmosphere. After the incubation, cells were washed once with 1 ml leucine-free medium, and 300 µl leucine-free medium with or without drug(s) were added to all wells. Toxins were then added in various dilutions including toxin free control. Final concentrations of toxins were 1-1000 ng/ml for ricin and DT, and 0.1-100 ng/ml for Stx and SLT-2. Cells were then incubated with gentle agitation for 3 h at 37 ^{o}C in a normal atmosphere. All wells were washed with 0.5 ml leucine-free medium once, and 200 µl leucine-free medium containing 2 µCi/ml [^{3}H]leucine was added. Cells were further incubated with gentle agitation for 20 min at 37 ^{o}C. The medium containing [^{3}H]leucine was then removed, 500 µl of 5% (w/v) TCA was added to all wells, and the plates were left on lab-bench for 10 min or stored in a refrigerator before proceeding next day. Washing with 5% (w/v) TCA was repeated twice. This ensured fixation of the cells in the plate and washing out of unincorporated [^{3}H]leucine. Finally, TCA was removed and proteins were dissolved in 200 µl/well of 0.1 M KOH. Samples from each well were transferred to separate counting vials, and 3 ml/vial of scintillation liquid Emulsifier-Safe™ was added and mixed well. The amount of [^{3}H]leucine in the samples was

counted by the liquid scintillation analyzer (Packard). Counts per minute (cpm) correspond to the amount of protein-incorporated [^{3}H]leucine in the cells. The relative protein synthesis (RPS) was estimated according to the equation: RPS = cpm(*sample*)/cpm(*control*).

2.2.3. Endocytosis of Biotin-Shiga Toxin

In order to be able to discriminate between cell-bound and internalized Shiga toxin, Shiga toxin, covalently linked to biotin (EZ-Link Sulfo-NHS-SS-Biotin, Pierce Biotechnology; the conjugation procedure was performed by J. Bergan in our department), was used in this assay. The conjugate biotin-Shiga toxin (biotin-Stx) has a disulfide bridge which can be reduced and thereby lead to cleavage of the conjugate. Sodium 2-mercaptoethanesulfonate (MESNa) was used as a reducing agent. MESNa does not pass the cell membrane and therefore acts only on the biotin-Stx present on the cell surface.

The detection system used for this assay is based on electrochemiluminescence. An electrochemiluminescent compound, ruthenium (II) trisbipyridine, was conjugated to a monoclonal antibody against Stx (Toxin Technology, 13C4; the conjugation procedure was performed by J. Bergan in our department). A schematic representation of the assay (Fig. 2.2) and a detailed explanation of the experimental procedure are given below.

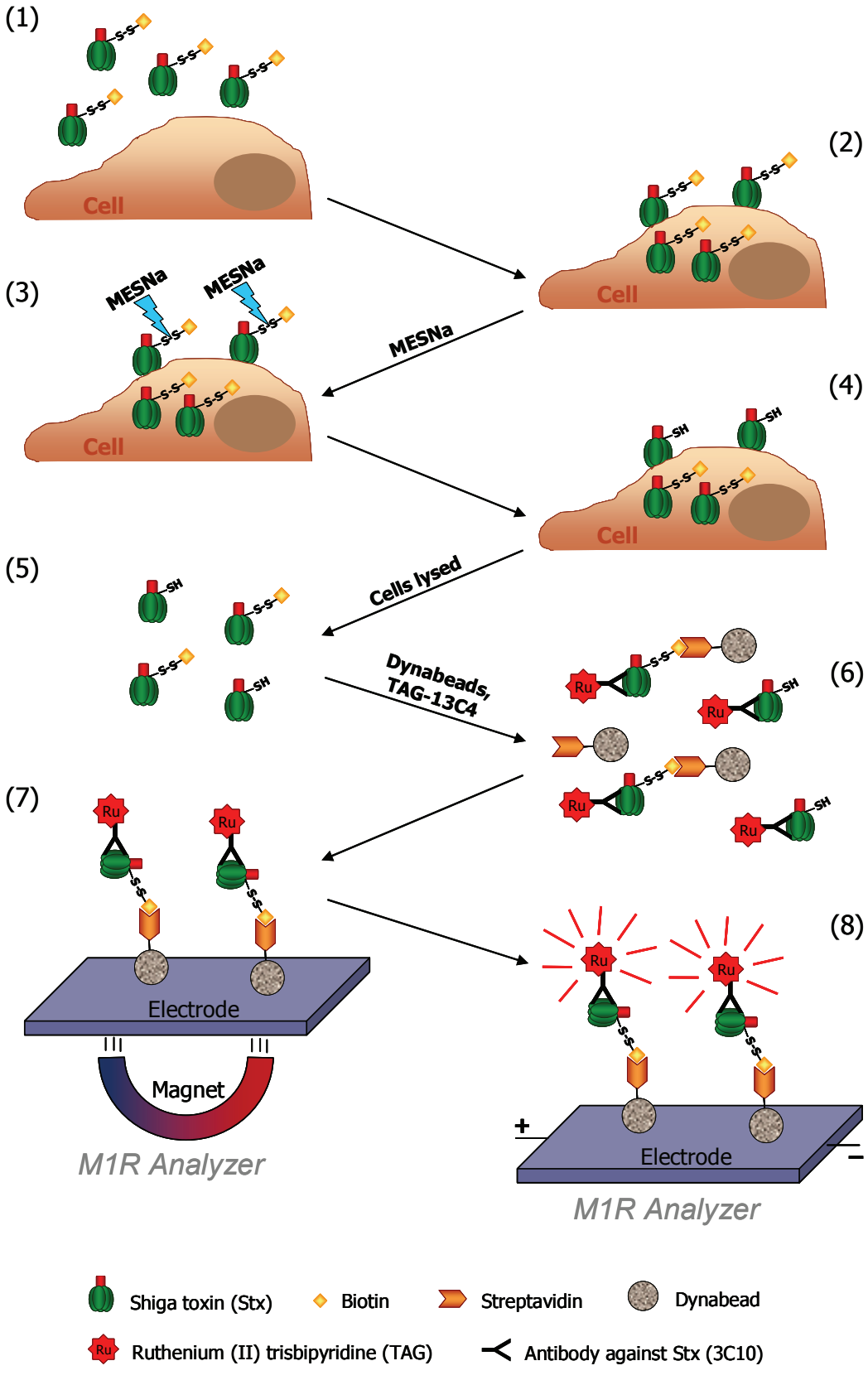

Fig. 2.2. Schematic representation of the endocytosis assay.

Cells were seeded in 24-well culture plates one day prior to the experiment. Seeding densities were 5 x 10^4 cells/well for short incubation experiments and 3 x 10^4 cells/well for long incubation (1-2 days) experiments. Next day, treatment with a particular drug was started and the cells were incubated at 37 ^oC in a 5% CO_2 atmosphere (this step not shown in the Fig. 2.2). The medium was removed and the cells were washed once with HEPES medium (37 ^oC). Biotin-Stx with the final concentration of 40 ng/ml was added to each well, and the plates were incubated with gentle agitation for 20 min at 37 ^oC in a normal atmosphere (steps 1-2 in the Fig. 2.2). Medium with biotin-Stx, which were not bound to or endocytosed by the cells, was removed, and all wells were washed with 1.6 ml ice-cold HEPES buffer (pH 8.6). Then, 300 µl freshly prepared 0.1 M MESNa solution was added to half of the plate, while rest of the wells were filled with 300 µl ice-cold HEPES buffer (pH 8.6). Plates were kept on ice for 30 min. MESNa breaks the sulfur bridge between the biotin and Stx and removes the biotin from biotin-Stx conjugates on the surface of the cell, while internalised biotin-Stx remain intact (steps 3-4 in the Fig. 2.2). After incubation, all wells were washed with 1.6 ml ice-cold HEPES buffer (pH 7.4) and 90 µl freshly made cell lysis solution was added. Plates were kept for 10 min on ice and then rotated for 10 s (step 5 in the Fig. 2.2). Then, 75 µl of cell lysate from each well were transferred to a 96-well plate (3 wells with 75 µl lysis solution were included as background wells). The solution of 0.5 µg/ml TAG-13C4 and 0.1 mg/ml dynabeads-streptavidin was prepared in assay diluent and distributed to each well (40 µl/well). The plate was wrapped in Parafilm and shaken at 400 rpm for 1.5 h with MS1 Minishaker (IKA) (step 6 in the Fig. 2.2). An additional 60 µl of assay diluent was pipetted to all wells, and the luminescence measured with the microplate reader (BioVeris) (steps 7-8 in the Fig. 2.2). The background counts from the wells without cells (only lysis solution) were subtracted from the counts of the sample wells during the mathematical analysis of the results.

To be able to normalise the endocytosis data according to the cell amount in the samples, 10 µl of the cell lysates were used for total protein measurement with the BCA method (detailed procedure explained in 2.2.1) and/or half of the 24-well plate was used for cell counting (explained in 2.2.1).

2.2.4. Quantitative Real Time RT-PCR

Cells were seeded in 6-well culture plates one day prior to the experiment if not stated otherwise. Seeding density, treatment and incubation time varied depending on the purpose of the experiment and are specified in the results part. Straight after the treatment, all wells were washed with sterile ice-cold PBS twice, plates wrapped with Parafilm and placed in freezer at -80 ^{o}C. Plates with frozen cells were stored at -80 ^{o}C until RNA isolation.

RNA isolation from cells

RNeasy Plus Mini Kit (QIAGEN) was used for purification of RNA from cultured cells. The kit is designed to purify RNA from small amounts of animal cells or tissues, with selective removal of double stranded DNA and enrichment for mRNA. Lysis buffer was added and pipetted up and down 15 times prior to transferring to sample tubes. The plate was kept on ice during this procedure. The tubes were centrifuged 18900 x g for 30 s to remove any foam, and placed into QIAcube (QIAGEN). For RNA purification, the protocol "Purification of total RNA from easy-to-lyse animal tissues and cells using gDNA Eliminator columns" (version 2, October 2007, QIAGEN) was used with 50 µl elution volume chosen. If not used immediately, samples with isolated RNA were stored at -80 ^{o}C.

Measuring RNA content in the samples

A small portion (4 µl) of the isolated RNA was diluted 1:18 in RNase-free (DEPC treated) water and kept on ice during whole procedure. Absorbance at wavelengths 230, 260 and 280 nm was registered with a GeneQuant pro spectrophotometer (GeneQuant), using a quartz cuvette with 10 mm path length. Distilled water was used as reference. The spectrophotometer displays RNA concentration in µg/ml and ratios of absorbance 260/230 (nucleic acids/salts) and 260/280 (nucleic acids/proteins). Samples were considered of sufficient purity if both ratios were above 1.5. In some experiments the RNA content was measured with a NanoDrop 2000 spectrophotometer (Thermo Scientific). The principle of measurement is similar to the one described earlier, but there was no need to dilute the sample, and a small volume (1-2 µl) of the sample was pipetted straight on the detector.

cDNA synthesis

iScript cDNA synthesis kit (Bio-Rad) was used for cDNA synthesis from the isolated RNA. The kit contains 5x reaction mixture (RNase inhibitors and a blend of oligo(dT) and random primers), RNase H^+ iScript reverse transcriptase and nuclease free water. RNase H^+ reverse transcriptases degrade RNA molecules present in RNA-DNA hybrids, ensuring a clean pool of cDNA. The 5x reaction mixture, reverse transcriptase and nuclease-free water were premixed in a sterile tube (referred as master-mix). The amount of RNA used for the reaction was 0.5 μg/tube, and appropriate volumes were added according to the measured RNA content of each sample. The components of the reaction were pipetted to the PCR tubes in the following order: nuclease-free water, master-mix and RNA. The final reaction volume was 20 μl/tube. One additional tube was prepared containing all components except for the reverse transcriptase, and it was used as a negative control for quantitative real-time RT-PCR and named -RT. cDNA synthesis was performed with a C1000 Thermal Cycler (Bio-Rad) using the procedure detailed in the Table 2.1.

Table 2.1. Protocol for cDNA synthesis.

Temperature	Time	Process
25 ^{o}C	5 min	Primer annealing
42 ^{o}C	30 min	cDNA synthesis
85 ^{o}C	5 min	Inactivation of enzymes
4 ^{o}C	Until stopped	Cooling

The lid was heated and set to 105 ^{o}C for the entire time of the run.

After the run, the cDNA was collected and frozen (-20 ^{o}C freezer) or kept on ice if used straight away.

Quantitative Real Time RT-PCR (qRT-PCR)

LightCycler 480 SYBR Green I Master kit (Roche), based on double stranded DNA binding fluorescent dye (SYBR Green I), was used for qRT-PCR. The kit contains PCR-grade water and 2x concentrated Master solution, consisting of FastStart Taq DNA polymerase, reaction buffer, dNTP mix and SYBR Green I dye. The master solution, water and the primers were pre-mixed in two separate RNAse-free tubes (master-mix). The first tube contained QuantiTect Primer Assay (QIAGEN) for Gb3 synthase gene (Gb3syn), while the second

contained forward and reverse primers (MWG-Biotech AG) for a housekeeping gene encoding TATA-binding protein (TBP). The TBP gene was used as a reference for relative quantification of Gb3syn expression. Finally, the template (cDNA, negative control –RT or PCR-grade water) was mixed with the prepared master mixes (in separate wells for Gb3syn and TBP) and distributed in 96-well PCR plates with two parallels of 20 µl for each. Serial dilutions of one cDNA sample were used for standard curve plotting. qRT-PCR was performed using LightCycler 480 (Roche) with the procedure detailed in the Table 2.2.

Table 2.2. Protocol for qRT-PCR.

Temperature	Time	Cycles	Process
95 ^{o}C	5 min	1	Preincubation
95 ^{o}C	10 s		
60 ^{o}C	20 s	45	Amplification
72 ^{o}C	10 s		
95 ^{o}C	5 s		
55 ^{o}C	1 min	1	Melting curve
97 ^{o}C	Continuous*		
40 ^{o}C	10 s	1	Cooling

* 0.11 ^{o}C/s rate.

Relative quantification of the ratio of Gb3syn/TBP was performed using LightCycler 480 software.

2.2.5. Immunofluorescence Confocal Microscopy

Live cell imaging

Cells (2 x 10^5 cells/dish) were cultured in 35 mm Petri dishes with 20 mm No. 1.5 coverglass (MatTek) one day before the experiment. Part of the medium was aspirated (leaving ~1 ml/dish) and dishes were placed on ice for 20 min to cool down. Primary antibody, anti-human Gb3, was diluted 50 times in ice-cold HEPES medium, and 250 µl/dish were added to aspirated dishes. Incubation proceeded for 1 h on ice. The cells were then washed three times for 3 min with ice-cold HEPES medium. Secondary antibody, rhodamine red X – anti-mouse, was diluted 100 times in ice-cold HEPES medium, and 250 µl/dish were added for

40 min on ice (kept in dark). Cells were washed again three times for 3 min with ice-cold HEPES medium. For nucleus staining, cells were incubated with 10 μg/ml Hoechst 33342 (Sigma) for 10 min at 37 ^{o}C and quickly placed back on ice.

Fluorescence images were acquired with the laser scanning microscope LSM 710 (Zeiss). Cells were kept at RT while microscoping, but no longer than 20 min/dish to reduce the possibility of antibody internalisation.

Fixed cell imaging

Cells were seeded in 6-well culture plates one day prior to the experiment. Each well contained three sterile round 10 mm No.1 microscope cover glasses. A subsequent experiment-specific treatment of the cells is explained in the result part. Cells were washed once with extensive amount of PBS and fixed in 10% (v/v) formalin solution (Sigma) for 15 min at RT. Formalin was aspirated and cells were washed three times for 5 min with PBS and then permeabilised with 0.1% (v/v) Triton X-100 solution in PBS for 5 min at RT. Cells were washed in PBS as previously described, and non-specific binding sites were blocked with 10% (v/v) fetal bovine serum in PBS (blocking solution) for 30 min at RT. Primary antibody, anti-human Gb3, was diluted 100 times in the blocking solution. Small drops (~20 μl) of diluted primary antibody were pipetted on a Parafilm sheet, and microscope slides with cells facing downwards were placed on them. Incubation proceeded for 1 h at RT or overnight at 4 ^{o}C. To avoid drying, cover slips were kept in a box with wet paper underneath. After the incubation, cover slips were placed in a 24-well plate, and the washing procedure was repeated. Secondary antibody, rhodamine red X – anti-mouse, was diluted 100 times in the blocking solution. Incubation with the secondary antibody was performed in the same way as for the primary antibody but for 30 min at RT in the dark. Cover slips were placed back in a 24-well plate, and the washing procedure was repeated. Finally, cover slips were carefully dried using a paper napkin, and mounted with ProLong Gold antifade reagent with DAPI (fluorescent probe for DNA), on microscopy slides. Slides were kept at 37 ^{o}C in dark overnight to allow the mounting solution to harden, and then stored at 4 ^{o}C.

Fluorescence images were acquired with the laser scanning microscope LSM 710 (Zeiss).

2.2.6. Time-Lapse Microscopy-Based Cell Migration Assay

Dish coating

In order to have a favourable surface for cell migration, 35 mm Petri dishes with 20 mm No. 1.5 coverglass (MatTek) were pre-coated with fibronectin or collagen prior to cell seeding. Dishes were pre-treated with 1 M HCl for 10 min at RT, and then washed with sterile PBS and sterile dist. water (this pre-treatment step is recommended by the producer to ensure optimal coating of the dish). Coating with fibronectin (20 μg/ml in water) was performed at 37 ^{o}C for 10 min. Surface coating concentration was 1 μg/cm^2. Several conditions were tested for collagen coating: two different collagen concentrations, 10 μg/cm^2 and 16 μg/cm^2, and two different diluents, 10 mM HCl and HEPES medium. Coating with the collagen was performed at RT overnight. Dishes were washed twice with HEPES medium after the coating, and, if the cells were not seeded straight away, the dish was filled with appropriate growth medium and stored at 4 ^{o}C, but no longer then for one day.

Cell growth

Cells (1.2 x 10^5 cells/dish) were seeded to freshly pre-coated dishes one or two days before imaging. The time and conditions for treatment with drugs or antibodies varied according to experimental purpose, and are explained in details in the results part.

Time-lapse microscopy

Time-lapse microscopy, a continuous imaging with constant time periods between pictures taken, was performed using Biostation IM (Nikon). The instrument is supplied with a red LED light source for phase contrast imaging. The long wavelength red light is considered to be cell-friendly and not produce any effect on cells even after several days of continuous imaging. An external light source Intensilight C-HGFIE (Nikon) and filter set 41002c TRITC (Chroma Technology) were used for fluorescence microscopy. The environment in the cell-chamber was kept humid and stable at 37 ^{o}C and 5% CO_2 during all time-lapse experiments.

In the start of time-lapse experiment, 15-20 observation points per dish were selected. The selections were chosen to have 5-10 cells/view and were distributed all over the

microscoping field of the dish. Time periods between pictures were 20 min if not stated otherwise, and total time-lapse experiment usually lasted for 20-24 h.

Immunofluorescence

In order to detect Gb3 present only on the cell surface, primary antibody, anti-human Gb3, diluted 50 times in warm (37 ^{o}C) growth medium was added to the aspirated dish straight after the time-laps experiment. Incubation with the antibody proceeded for 30 min. Cells were washed three times with warm complete growth medium and fixed with 10% (v/v) formalin solution for 10 min. Then formalin solution was aspirated, cells were washed as explained previously and permeabilised with 0.1% (v/v) Triton X-100 solution in PBS for 5 min. Washing was repeated, and secondary antibody, rhodamine red X – anti-mouse, diluted 100 times in complete growth medium was added. Incubation with secondary antibody proceeded for 30 min before cells were washed again.

When the total pool of Gb3 in the cells was the object for detection, cells were fixed and permeabilised immediately after the time-lapse experiment. Subsequently, the samples were incubated with primary and secondary antibodies as described in the previous section.

All steps of immuno-staining were performed at 37 ^{o}C in a 5% CO_2 atmosphere (in the Biostation cell-chamber). Fluorescence images were acquired by Biostation IM (Nikon) using exactly the same observation points as for the time-lapse experiment.

Data analysis

Randomly chosen cells (5-10 from each observation point) were manually tracked using ImageJ software. The tracking was stopped if the cell started to divide. Chemotaxis and Migration Tool (Ibidi) – a plugin for the ImageJ software – was used to quantify cell migration parameters: velocity, directionality, accumulated distance and Euclidean distance.

The quantification of fluorescence was performed using ImageJ software.

2.2.7. Statistical data analysis

Standard error of mean (SEM) was used to plot the error bars for results obtained from experiments repeated at least three times. SEM represents a standard deviation of the mean and shows how far the estimated mean value is likely to be from the true mean of a given population. SEM was calculated according to the following formula: $SEM = s/\sqrt{n}$; s – standard deviation of the sample, n – the number of independent experiments. For the experiments repeated only twice, $|x-\mu|$ was used for plotting the error bars; x – value obtained from one of experiments, μ – mean value calculated from both experiments. $|x-\mu|$ represents a distance between the mean value and values obtained from two independent experiments.

Two sample Student's t-test was used to estimate if the difference between two mean values was significant. The mean values were considered statistically different if p value for the Student's t-test was lowers than 0.05.

The linear fitting of the data was performed using Originpro 8 software. The coefficient of determination (r^2) is calculated as a square of the correlation coefficient, and represents the proportion of common variation in the two variables (for example, $r^2 = 0.5$ means, that 50% of the variance in X can be explained by variation in Y) [127]. Therefore r^2 was used to estimate the strength of correlation between two parameters measured.

3. Results

3.1. The expression of Gb3 synthase gene in HEp-2 cells

In this study, we used a quantitative real time RT-PCR (qRT-PCR) technique to investigate the expression of Gb3 synthase gene (Gb3syn) in cultured cancer cells. For the relative quantification of Gb3syn mRNA levels in the samples, a housekeeping gene encoding TATA binding protein (TBP) was used as a reference. The C_p values (threshold crossing points) for the TBP remained constant within treated and control samples.

2DG inhibits Gb3syn expression in HEp-2 cells

2DG was recently reported to inhibit Gb3syn expression in HeLa cells (Gb3syn promoter activity was measured indirectly using a reporter vector) [45]. To study if 2DG had a similar inhibitory effect on Gb3 synthesis in HEp-2 cells, we subjected HEp-2 cells to 10 mM 2DG for various time periods prior to extraction of mRNA, and performed qRT-PCR according to the procedure described in 2.2.4. A significant reduction in Gb3syn expression was observed after 4 h and 6 h of the 2DG treatment (Fig. 3.1 A), with the highest decrease (40%) in Gb3syn/TBP ratio at the 6 h time point, compared to untreated (control) cells (Fig. 3.1 C). However, the level of mRNA for Gb3syn was back to that of the control cells after 48 h of the incubation (Fig. 3.1 C).

It was earlier demonstrated by Kijimoto and Hakomori that Gb3syn expression depended on cell density and increased with higher cell confluency in the culture of non-transformed cells [128]. This was also observed in this study (Fig. 3.1 A). The level of mRNA for Gb3syn increased 2.5 folds when cell culture density changed from ~30% at 1 h to ~80% at 48 h (the cell confluency was estimated visually according to dish surface covering; the increase in cell number is presented in Fig. 3.1 B). However, the same increase in Gb3syn expression was also observed in 2DG treated samples, though cell growth was partly inhibited by the treatment, and cells reached only ~50% confluency after 48 h (Fig. 3.1 B).

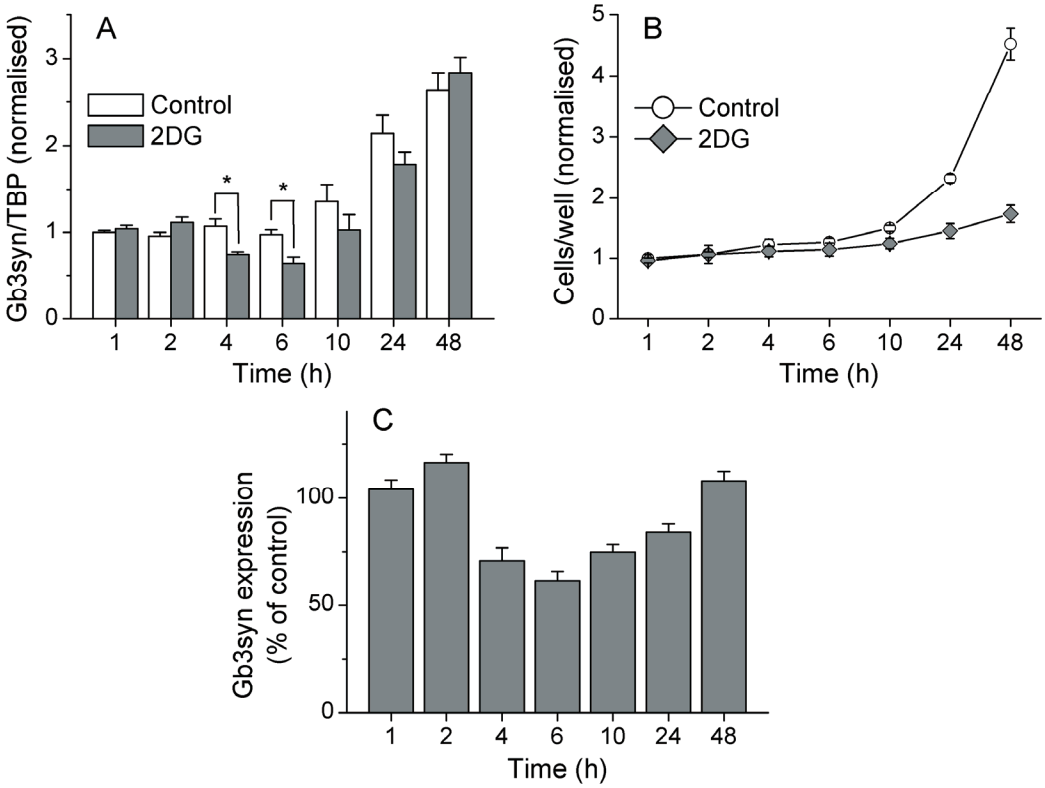

Fig. 3.1. Gb3syn expression in HEp-2 cells. HEp-2 cells were treated with 10 mM 2DG for various time periods, total mRNA was isolated from treated and control (untreated) cells, and Gb3syn expression was measured by qRT-PCR. TBP gene was used as a reference for relative quantification. (A) Gb3syn/TBP values were normalised to the corresponding control at the 1 h time point. Values for Student's t-test *p < 0.05. (B) Cells were counted in control and 2DG-treated wells (performed in parallel to mRNA isolation). The cell number was normalised to the control value at 1 h (C) The Gb3syn expression of 2DG treated samples was calculated relative to the untreated control samples. The results are plotted as mean values ± SEM of three independent experiments.

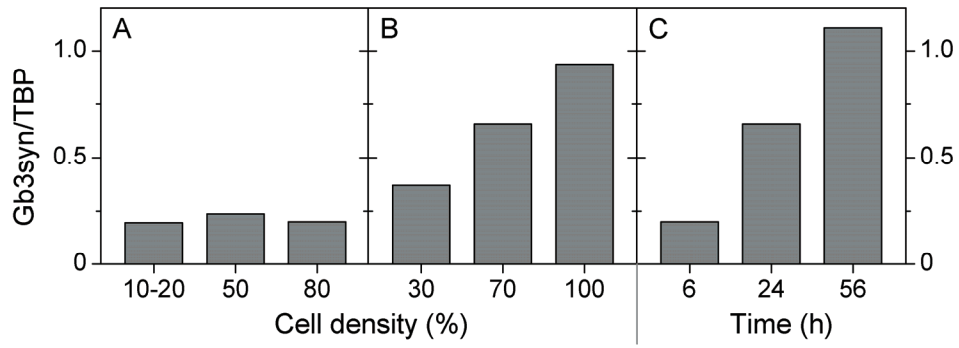

Fig. 3.2. Cell density and time of growth-induced changes in Gb3syn expression in HEp-2 cells. HEp-2 cells were seeded in culture dishes with various cell numbers and subjected to RNA extraction after different time periods (time counted from the moment of cell seeding). The cell density was estimated visually using a phase contrast light microscope, and presented as a percentage of dish surface coverage by cells. Gb3syn expression was measured by qRT-PCR, and TBP was used as a reference gene for relative quantification. Plotted: Gb3syn/TBP ratios in cells, which had reached different densities within (A) 6 h and (B) 24 h after cell seeding, and (C) in cells, which were of similar density (70-80%), but were grown in the culture dish for different time periods.

Gb3syn expression in HEp-2 cells is cell context dependent

Since we found that Gb3syn expression was increased not only in control, but also in 2DG-treated cells (which were growing much slower and were of lower density), we investigated if Gb3syn expression was dependent on time which the cells had spent in the culture. To study this, HEp-2 cells were seeded in culture dishes at different starting densities, and mRNA was extracted after various time periods. To analyse the effect of cell density, the Gb3syn/TBP ratios were compared between the samples from cells with different densities after the same culturing time (Fig. 3.2 A, B), while samples from cells with similar cell density, but different in the time of growth, were compared to each other to investigate the contribution of timing (Fig. 3.2 C). Although the results are preliminary, it is clear that both cell density and time of growth were affecting the expression of Gb3syn in HEp-2 cells, and in both cases the Gb3syn was upregulated in response to higher cell density and longer time spent in the culture dish. Six hours after seeding, cells were fully attached to the dish surface, but there was yet no difference in Gb3syn expression between sparsely and densely seeded cells (Fig. 3.2 A). However, in cells which had been growing for 24 h in the culture, Gb3syn expression was 2.5 times higher in confluent cells than in cells which were growing sparsely (Fig. 3.2 A). Furthermore, the Gb3syn expression measured in cells which all had reached 70-80% density, but had been growing in the dish for 6 h, 24 h or 56 h after seeding, was increased in cells grown for longer time periods, and within 56 h was 5 times and 1.4 times higher than that at the 6 h and 24 h time points, respectively (Fig. 3.2 C).

3.2. 2-deoxy-D-glucose induced protection against protein toxins

To confirm that 2DG had a specific effect on Gb3 synthesis, cell intoxication by four protein toxins, Shiga toxin (Stx), Shiga-like toxin 2 (SLT-2), Diphtheria toxin (DT) and the plant toxin ricin, was tested. Gb3 serves as a receptor for Stx, SLT-2 and ricin (it must be noted that ricin binds to both glycoproteins and glycolipids with terminal galactose), but not for DT, which binds to the heparin-binding epidermal growth factor precursor (pro-HB-EGF) [97]. All the toxins inhibited protein synthesis during cell intoxication. Therefore, the remaining cellular protein synthesis was used to asses the efficiency of the intoxication.

2DG protects against Stx and DT, but not against ricin

HEp-2 cells were treated with 10 mM 2DG for 24 h prior to addition of increasing concentrations of a given toxin. Then, cells were incubated with [^{3}H]leucine containing growth medium, and incorporated [^{3}H]leucine was measured. The results showed, that 2DG-treated HEp-2 cells were 40 times less sensitive to Stx and 30 times less sensitive to DT (Fig. 3.3 A, D). Preliminary data also indicated that 2DG treatment induced protection against SLT-2 to an even greater extent (Fig. 3.3 C). However, 2DG treatment had no effect on cell intoxication by ricin (Fig. 3.3 B).

The protective effect of 2DG against Stx and SLT-2 may be an outcome of decreased levels of surface Gb3, since cellular level of Gb3 has been shown to be reduced in teratocarcinoma cells after 2DG treatment [45]. However, a lowered number of Gb3 on the cell surface can not explain reduced cell sensitivity to DT. Therefore, we tested if cell protection could be caused by cell deprivation of ATP, which is required for the receptor-mediated endocytosis of the toxins.

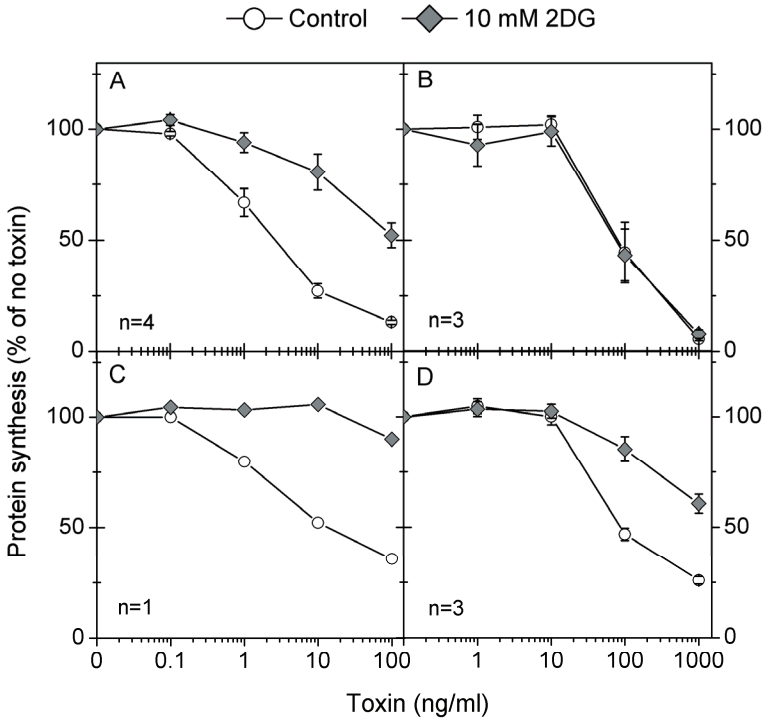

Fig. 3.3. The effect of 2DG on HEp-2 cell sensitivity to bacterial and plant toxins. HEp-2 cells were cultured with or without (control) 10 mM 2DG for 24 h. The cells were then incubated for 3 h with increasing concentrations of (A) Stx, (B) ricin, (C) SLT-2 or (D) DT. Finally, incorporated [^{3}H]leucine was measured to determine remaining cellular protein synthesis. Protein synthesis was calculated as a percentage of samples without toxin treatment, and plotted as mean values ± SEM; n, the number of independent experiments.

Pyruvate does not restore HEp-2 cell sensitivity to Stx and DT

The most profound effect of 2DG on cells might be depletion of ATP caused by a glycolysis inhibition. Medium supplementation with pyruvate has been demonstrated to partly recover ATP yield in bovine pulmonary artery endothelial cells treated with 2DG [129]. To test if depletion of ATP in HEp-2 cells accounted for the 2DG-induced protection against Stx and DT, the cells were treated with 10 mM 2DG, 10 mM sodium pyruvate, or the combination of these compounds for 4 h or 24 h. Cells were then incubated for 3 h with increasing concentrations of the toxins, and incorporated [^{3}H]leucine was measured.

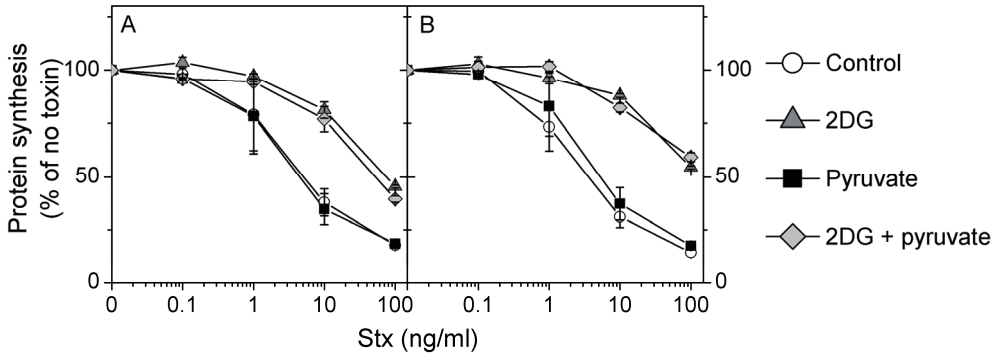

4 h		*24 h*		
IC_{50}, ng/ml	Protection	IC_{50}, ng/ml	Protection	
5.1 ± 2.7	–	3.7 ± 1.5	–	Control
74 ± 5	19 ± 9	> 100	43 ± 15 *	10 mM 2DG
4.7 ± 2.4	0.93 ± 0.02	5.5 ± 2.5	1.5 ± 0.1	10 mM pyruvate
52 ± 9	13 ± 5	> 100	110 ± 75 *	2DG + pyruvate

** Approximate values, because IC_{50} of these samples were higher then 100 ng/ml and were out of the investigation range.*

Fig. 3.4. HEp-2 cell sensitivity to Stx after 2DG and/or sodium pyruvate treatment. HEp-2 cells were treated with 10 mM 2DG and/or 10 mM sodium pyruvate for (A) 4 h or (B) 24 h prior to incubation with increasing concentrations of Stx for 3 h. Incorporated [^{3}H]leucine was then measured, and protein synthesis was calculated as a percentage of the samples, which were not treated with the toxin. Results are plotted as mean values ± |x-μ| of two independent experiments. The table: IC_{50}, concentration of the toxin which inhibited protein synthesis by 50%. Protection, the ratio between IC_{50} of 2DG or/and sodium pyruvate-treated sample and IC_{50} of the control. The values listed are means ± |x-μ| of two independent experiments.

The protection against Stx after 4 h incubation with 2DG was almost 20-fold and increased up to more than 40-fold with longer incubation time (24 h) (Fig. 3.4). In contrast, a short 4 h incubation with 2DG induced only a slight (less then 2-fold) protection against DT, and a long incubation time (24 h) was needed to protect cells from DT (Fig. 3.5). Sodium pyruvate

alone did not affect HEp-2 cell sensitivity to Stx and DT, and when pyruvate was added in combination with 2DG the cell protection against Stx was still at the same level as in cells treated with 2DG alone (Fig. 3.4). However, although the IC_{50} values were not significantly different between samples treated with 2DG or with a combination of 2DG and sodium pyruvate, there was a significant rescue in cell sensitivity to DT when 24 h incubation with drugs was followed by the addition of 100 ng/ml toxin (Fig. 3.5). This indicates that mechanisms responsible for cell protection against Stx and DT by 2DG are at least partially different, and ATP depletion is involved in protection against DT, while protection against Stx is ATP-independent.

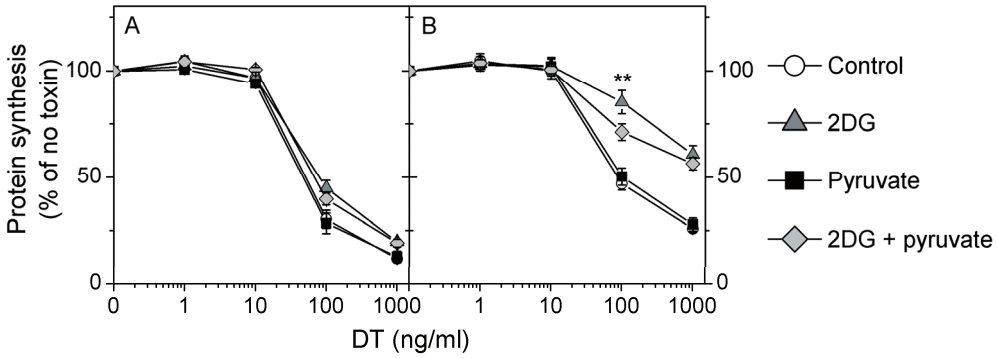

4 h		*24 h*		
IC_{50}, ng/ml	Protection	IC_{50}, ng/ml	Protection	
52 ± 7	–	93 ± 15	–	Control
84 ± 15	1.6 ± 0.1	> 1000	32 ± 10 *	10 mM 2DG
49 ± 6	0.93 ± 0.03	127 ± 30	1.3 ± 0.3	10 mM pyruvate
69 ± 5	1.4 ± 0.1	> 1000	38 ± 17 *	2DG + pyruvate

** Approximate values, because IC_{50} of these samples were higher then 1000 ng/ml and were out of the investigation range.*

Fig. 3.5. HEp-2 cell sensitivity to DT after 2DG and/or sodium pyruvate treatment. HEp-2 cells were treated with 10 mM 2DG and/or 10 mM sodium pyruvate for (A) 4 h or (B) 24 h prior to incubation with increasing concentrations of DT for 3 h. Incorporated [^{3}H]leucine was the measured, and protein synthesis was calculated as a percentage of the samples, which were not treated with the toxin. Results are plotted as mean values ± SEM of three independent experiments. Value for Student's t-test **$p < 0.05$. The tables: IC_{50}, concentration of the toxin which inhibited protein synthesis by 50%. Protection, the ratio between IC_{50} of 2DG or/and sodium pyruvate-treated sample and IC_{50} of the control. The values listed are means ± SEM of three independent experiments.

Protection against Stx by 2DG in different cells

In addition to HEp-2 cells, two colon cancer cell lines, SW480 and HT-29, were tested for sensitivity to Stx. The HEp-2 cells and HT-29 cells showed similar sensitivity to Stx, while SW480 was found to be 10 times less sensitive to the toxin (Fig. 3.6). To test if protection against Stx caused by 2DG treatment is not restricted to HEp-2 cells, all three cell lines were treated with 10 mM 2DG for 24 h prior to the addition of increasing concentrations of Stx. A decreased sensitivity to Stx after 2DG treatment was observed in all cells. The HEp-2 and HT-29 cells were protected more then 50 times against Stx, while SW480 showed lower, but still high (~20-fold) protection against Stx after 24 h incubation with 2DG (Fig. 3.6).

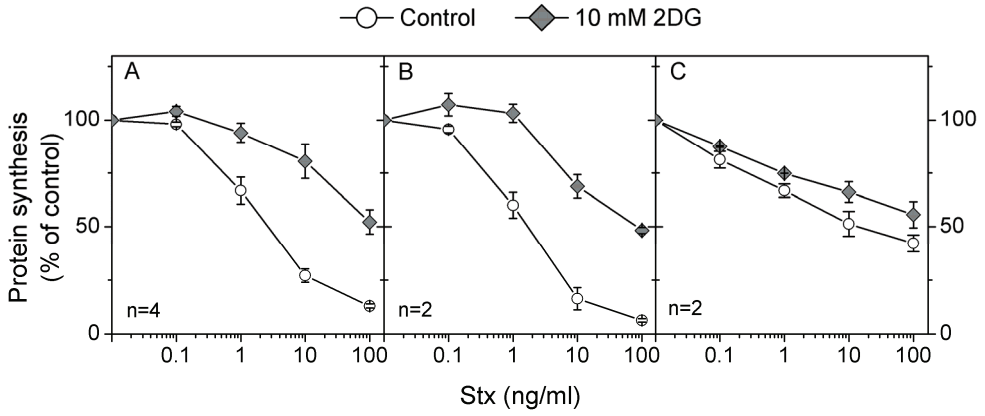

HEp-2		*HT-29*		*SW480*		
IC_{50}, ng/ml	Protection	IC_{50}, ng/ml	Protection	IC_{50}, ng/ml	Protection	
2.7 ± 0.7	–	1.7 ± 0.6	–	25 ± 19	–	Control
> 100	> 50	87 ± 10	> 50	> 100	20 ± 5 *	10 mM 2DG

** Approximate values, because IC_{50} of these samples were higher then 100 ng/ml and were out of the investigation range.*

Fig. 3.6. Protection against Stx by 2DG. (A) HEp-2, (B) HT-29 and (C) SW480 cells were treated with 10 mM 2DG for 24 h. Both treated and untreated (control) cells were then incubated for 3 h with increasing concentrations of Stx, and incorporated [^{3}H]leucine was measured. Protein synthesis was calculated as a percentage of the samples without toxin treatment. Results are plotted as mean values ± SEM of four independent experiments for HEp-2 cells, and as mean values ± |x-μ| of two independent experiments for HT-29 and SW480 cells. The table: IC_{50}, concentration of the toxin which inhibited protein synthesis by 50%. Protection, the ratio between IC_{50} of a 2DG treated sample and IC_{50} of the control. The listed values represent means ± SEM for HEp-2 cells, and means ± |x-μ| for HT-29 and SW480 cells.

2DG does not affect Stx endocytosis in HEp-2 cells

The data shown above demonstrated that 4 h and 6 h incubation with 10 mM 2DG significantly decreased the expression of Gb3syn, which should lead to decreased Gb3 synthesis and reduced Gb3 levels in the cells. To test, if 2DG treatment reduced the binding and/or endocytosis of Stx and thus led to cell protection against the toxin, the binding and endocytosis of Stx was measured as described in 2.2.3. HEp-2 cells were pre-treated with 10 mM 2DG for 4 h or 24 h prior to addition of biotin-Stx. Interestingly, there was no significant change observed in total binding of biotin-Stx after either 4 h or 24 h treatment with 2DG (Fig. 3.7 A). Furthermore, the decrease in the endocytosed proportion of the labelled toxin was less then 10% and was not significant after 4 h or 24 h incubations with 2DG (Fig. 3.7 B). Therefore, neither decreased binding, nor inhibited endocytosis of Stx could explain the 2DG-induced cell protection.

The control experiments were preformed on ice to test if MESNa treatment was sufficient to cleave biotin from the biotin-Stx bound to the cell surface. The plate with cells was placed on ice for 20 min and then ice-cold HEPES medium containing biotin-Stx was added for 30 min. The subsequent steps were performed according to the protocol given in 2.2.3. The counts measured from the wells which were treated with MESNa were lower than 10 % of the total binding. This was considered as the background level and was similar for all three cell lines used in this study.

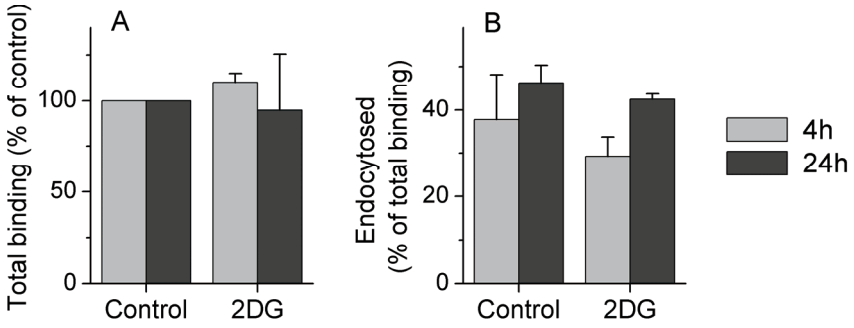

Fig. 3.7. Biotin-Stx endocytosis in control and 2DG treated HEp-2 cells. HEp-2 cells were incubated with 10 mM 2DG for 4 h or 24 h prior to the addition of biotin-Stx construct. One half of the wells was then treated with MESNa solution to remove biotin from the cell surface-bound biotin-Stx. Finally, cells were lysed, and intact biotin-Stx was quantified. The number of cells was measured in parallel plates and all counts were normalised to cell number (counts/cell). (A) Total biotin-Stx binding, calculated as a percentage of untreated control. (B) The endocytosed population of biotin-Stx, calculated as a percentage of the total binding in a given sample. The results are plotted as mean values ± $|x-\mu|$ of two independent experiments.

3.3. Cell sensitisation to Shiga toxin by sodium butyrate

In contrast to 2DG, which has been found to protect cells against Stx, sodium butyrate is known to sensitise cells to Stx. It was first demonstrated by Sandvig *et al.* [94] that cells which normally were resistant to Stx became sensitive after treatment with butyric acid. To test the sensitising effect of sodium butyrate on colon cancer cells, SW480 and HT-29 cells were treated with 0.5 mM, 1 mM or 2 mM sodium butyrate for 48 h prior to addition of increasing concentrations of Stx. Then, cells were incubated with [^{3}H]leucine containing growth medium, and incorporated [^{3}H]leucine was measured. The results showed that even the lowest concentration of sodium butyrate (0.5 mM) sensitised SW480 cells to Stx more than 80 times (Fig. 3.8 A). The effect on HT-29 cells was lower, and at the highest a 6-fold sensitisation was observed after treatment with 2 mM sodium butyrate (Fig. 3.8 B). Interestingly, though HT-29 cells were much more sensitive to Stx than SW480 cells in control conditions (there was a 10-fold difference between IC_{50} values), sodium butyrate treatment sensitised SW480 cells to Stx to a much higher extent than HT-29 cells (Fig. 3.8).

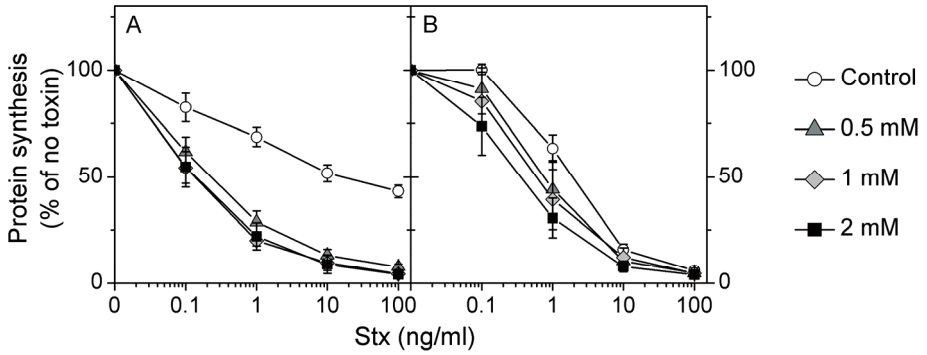

SW480		*HT-29*		
IC_{50}, ng/ml	Sensitisation	IC_{50}, ng/ml	Sensitisation	
24 ± 16	–	1.9 ± 0.5	–	Control
0.2 ± 0.1	85 ± 33	1 ± 0.5	2.6 ± 1.0	0.5 mM butyrate
0.1 ± 0.1	> 100	0.8 ± 0.5	3.3 ± 1.3	1 mM butyrate
0.1 ± 0.1	>100	0.4 ± 0.2	5.9 ± 1.9	2 mM butyrate

Fig. 3.8. Sensitisation to Stx by sodium butyrate. (A) SW480 and (B) HT-29 cells were treated with sodium butyrate for 48 h prior to the addition of Stx for 3 h, and incorporated [^{3}H]leucine was then measured. Protein synthesis was calculated as a percentage of the samples without toxin. Results are plotted as mean values ± |x-μ| of two independent experiments. The table: IC_{50}, the concentration of Stx, which inhibited protein synthesis by 50%. Sensitisation, the ratio between IC_{50} of the control sample and IC_{50} of the sodium butyrate-treated sample. The listed values represent means ± |x-μ|.

Effect of sodium butyrate on binding and endocytosis of Stx

To test if cell sensitisation to Stx by sodium butyrate is related to increased binding and/or internalisation of the toxin, SW480 and HT-29 cells were treated with 0.5 mM or 2 mM sodium butyrate for 48 h prior to the addition of biotin-Stx. The detailed procedure used to assess the binding and the endocytosis of biotin-Stx is given in 2.2.3.

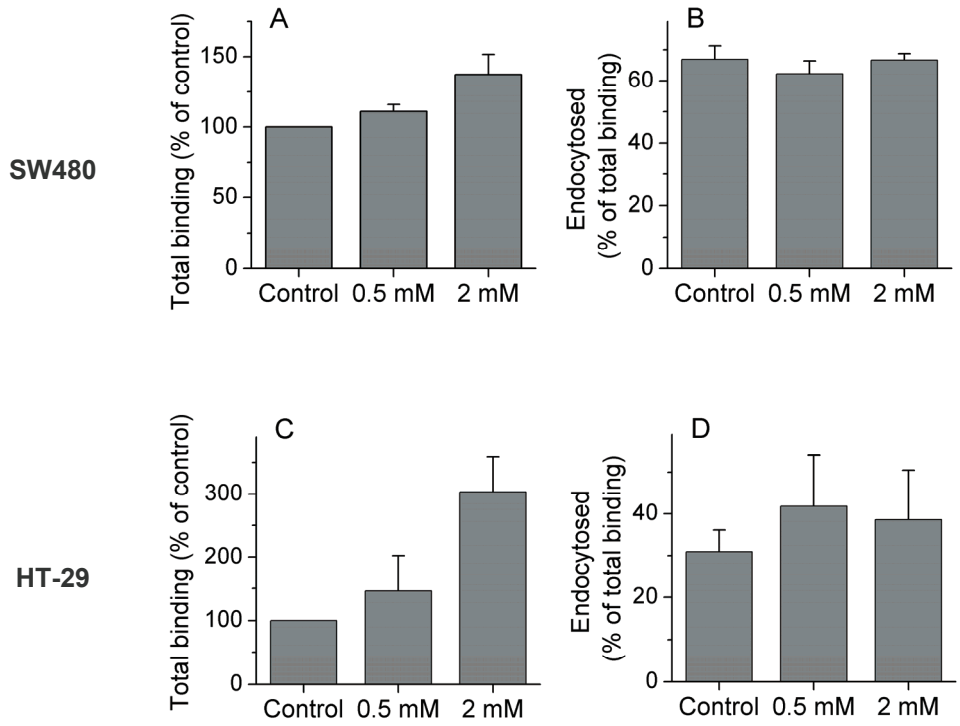

Fig. 3.9. Biotin-Stx endocytosis in control and sodium butyrate-treated colon cancer cells. SW480 (top) and HT-29 (bottom) cells were treated with 0.5 mM or 2 mM of sodium butyrate for 48 h prior to the addition of biotin-Stx. One half of the wells were then treated with MESNa solution to remove biotin from the cell surface-bound biotin-Stx. Finally, the cells were lysed, and intact biotin-Stx was quantified. The number of cells was measured in parallel plates and all counts were normalised to cell number (counts/cell). (A,C) The total biotin-Stx binding, calculated as a percentage of the binding to untreated control cells. (B,D) The endocytosed population of the biotin-Stx, calculated as a percentage of the total binding in a given sample. The results are plotted as mean values ± |x-μ| of two independent experiments.

Sodium butyrate concentration-dependent increase in the total binding of biotin-Stx was observed in both SW480 and HT-29 after two days of butyrate treatment (Fig. 3.9 A, C). However, endocytosis of the labelled toxin was not affected by the treatment, and the same proportion of biotin-Stx was endocytosed by control and butyrate-treated cells (Fig. 3.9 B, D). In contrast to cell sensitisation to Stx by sodium butyrate, where 0.5 mM concentration of butyrate was sufficient to increase SW480 cell sensitivity to Stx 80 times, the same

treatment did not significantly change the total binding of biotin-Stx, suggesting that sensitisation to Stx was not related to increased number of Stx molecules entering the cell. However, the increased binding of Stx could be the reason for HT-29 sensitisation to Stx by sodium butyrate, since the total binding of biotin-Stx was increased 3 times after 2 mM sodium butyrate treatment (Fig. 3.9 C). These results suggest that different mechanisms could be involved in SW480 and HT-29 sensitisation to Stx by sodium butyrate.

3.4. The effect of sodium butyrate on Gb3 synthase gene expression in colon cancer cells

Since it was observed that sodium butyrate treatment sensitised SW480 and HT-29 cells to Stx and increased biotin-Stx binding, the effect of butyrate on Gb3syn expression in these cells was tested. The cells were pre-treated with 1 mM sodium butyrate for different time periods prior to extraction of mRNA, and qRT-PCR was performed according to the protocol described in 2.2.4. In SW480 cells, a significant 5-fold increase in Gb3syn expression was observed 24 h after sodium butyrate treatment, and the expression also increased slightly after even longer incubation (Fig. 3.10 A, C). The same tendency was observed in HT-29 cells, but the increase in Gb3syn expression was only half that in SW480 cells (Fig. 3.10 D, F). The growth of both cell lines was inhibited slightly by sodium butyrate treatment (Fig. 3.10 B, E).

Contrary to what was shown for HEp-2 cells, Gb3syn expression was not upregulated in response to higher cell density in SW480 and HT-29 cells (Fig. 3.10 A, D). This could be due to weak cell-to-cell contacts in SW480 culture, since these cells did not form well defined colonies. However, HT-29 cells formed compact colonies in the dense culture, but still there was no regulation of Gb3syn expression observed. The lack of Gb3syn upregulation in response to cell culture density by SW480 and HT-29 cells is in agreement with published data showing that the cell density-dependent regulation of glycosphingolipid synthesis is lost during malignant cell transformation [128;130]. However, it should be noted that HEp-2 cells are also cancer cells, but the expression of Gb3syn was upregulated in response to increased cell culture density in these cells (Fig. 3.2 B).

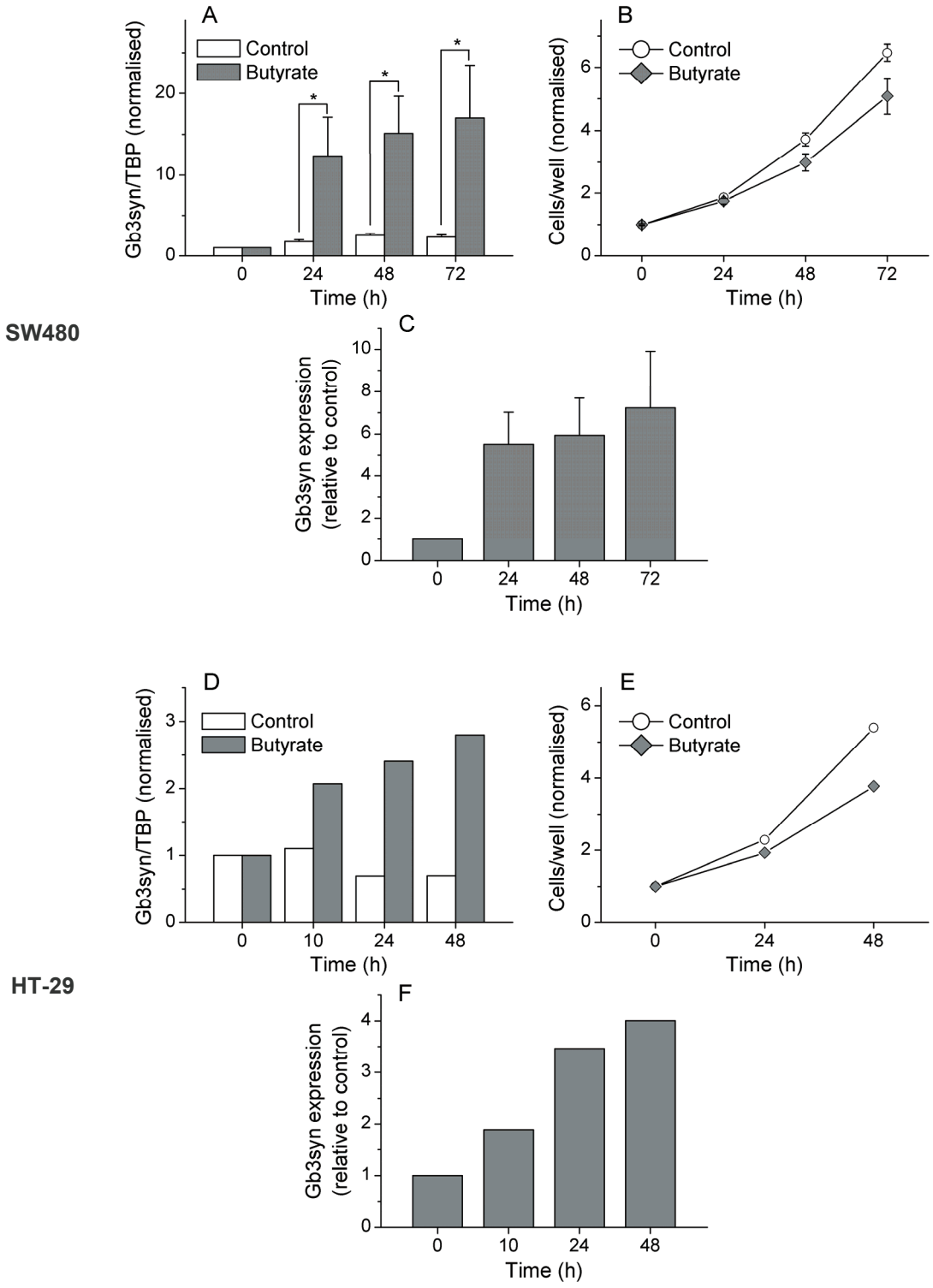

Fig. 3.10. Gb3syn expression in colon cancer cells. SW480 (top) and HT-29 (bottom) cells were treated with/without 1 mM sodium butyrate for various time periods. Then, total mRNA was isolated, and Gb3syn expression was measured by qRT-PCR. TBP was used as a reference gene for relative quantification. (A,D) Gb3syn/TBP values normalised to the corresponding control at the 0 h time point. (B,E) The cell number in treated and control wells, normalised to the control value at the 0 h time point. (C,F) Gb3syn expression in sodium butyrate-treated samples calculated relatively to the untreated controls. For SW480 cells results are plotted as mean values ± SEM of three independent experiments. Values for Student's t-test *$p < 0.05$. For HT-29 cells preliminary data from one experiment is shown.

3.5. The effect of sodium butyrate on the cell cycle

Sodium butyrate has been reported to induce cell cycle arrest in G2 phase in normal and cancer cells [131-133]. To study if sodium butyrate interfered with the cell cycle in SW480 cells, we analysed phase contrast images of SW480 cells pre-treated with/without 0.5 mM sodium butyrate prior to the time-lapse imaging. All the cells in the field of view were assigned to one of the groups: (i) containing a single nucleus, (ii) containing two nuclei or (iii) containing three or more nuclei. The results showed that 8% of sodium butyrate-treated cells contained more than one nucleus, while only 4% of such cells were observed in the control group. Furthermore, the percentage of binucleated cells was similar in the control and sodium butyrate-treated samples, but a proportion of polynucleated cells was significantly increased in the sodium butyrate-treated group compared to the control (Fig. 3.11 A). The observations also indicated that some of the sodium butyrate-treated cells were unable to finish cytokinesis and fused back forming binucleated cells (Fig. 3.11 B). In agreement with published data [132;133], binucleated cells were still able to reinitiate cell cycle (without cytokinesis), which led to doubled number of nuclei and increased cell size (Fig. 3.11 C).

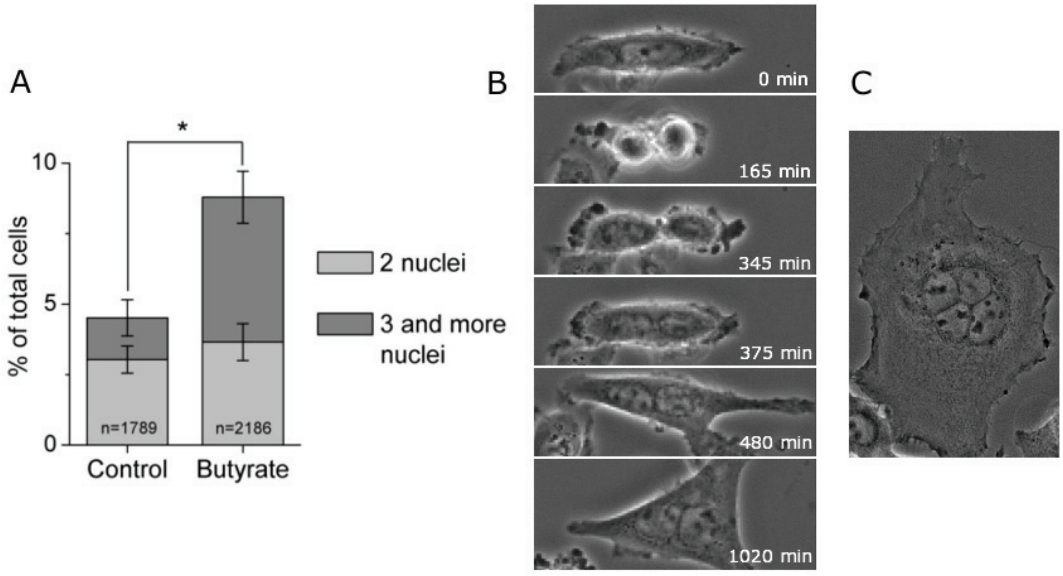

Fig. 3.11. The increase in polynucleated cells after sodium butyrate treatment. SW480 cells were cultured normally (Control), or with 0.5 mM sodium butyrate added to growth medium for 48 h (Butyrate). Then, phase contrast images were taken and analysed. (A) The number of cells which contained 2 or more nuclei was calculated as a percentage of total cells. The results are plotted as mean values ± SEM of five independent experiments; n, number of cells analysed. Value for Student's t-test *$p < 0.05$. (B) The time series of phase contrast images showing an unsuccessful division of a SW480 cell grown in medium supplemented with 0.5 mM sodium butyrate. (C) The phase contrast image of the cell containing four nuclei.

3.6. The detection of Gb3 by immunofluorescence in live and fixed cells

It has been suggested that not all Gb3 present on the cell surface is available for the binding by Stx or anti-Gb3 antibodies, since the orientation of the carbohydrate part might be dependent on the concentration of cholesterol and the presence of other GSLs in the membrane, and also membrane proteins may inhibit the binding [86;134]. In this study it was tested if the mouse IgM anti-Gb3 antibody (supplied by BD Pharmingen) could be used to detect Gb3 present on the cell surface. The cells were cooled on ice prior to addition of ice-cold HEPES medium containing the antibody, and kept on ice during the whole labelling procedure, except for a short 10 min incubation with Hoechst at 37 ^{o}C for nucleus staining. The confocal fluorescence imaging was performed at room temperature, but only for short time intervals to avoid warming of the samples.

Gb3 present in the plasma membrane was detected in all cells tested, but the proportion of positively labelled cells differed between the cell lines. All HEp-2 cells were found to be positive for Gb3 (Fig. 3.12 A). A majority (~70%) of the HT-29 cells was detected to be positively labelled for Gb3 (Fig. 3.12 B), while less than 10% of SW480 cells had Gb3 detected by the immunofluorescence microscopy (Fig. 3.12 C). It has been demonstrated earlier by Kovbasnjuk *et al.* [8] that colon cancer cells have different amounts (or different pools) of Gb3 presented on the cell surface. In agreement with our observation, 90% of HT-29 cells have been found to be positive for Gb3 when stained live with fluorescently labelled StxB [8].

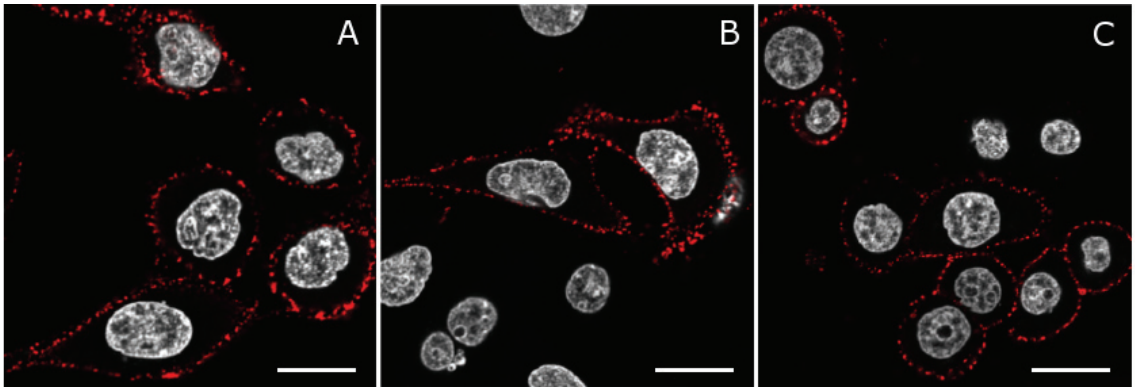

Fig. 3.12. Detection of surface Gb3 in live cells by immunofluorescence microscopy. (A) HEp-2, (B) SW480 and (C) HT-29 cells were labelled on ice with mouse anti-Gb3, followed by rhodamine red X conjugated anti-mouse IgG (red). Nuclei were stained with Hoechst 33342 (grey). Scale bars, 20 μm.

Since we found that only a few live SW480 cells were labelled with the anti-Gb3 antibody, we tested if higher amount of Gb3 could be detected in formalin-fixed and Triton X-100-permeabilised cells. The 10% (v/v) formalin solution both fixed and partially permeabilised the cells, which made it possible to label intracellular Gb3, whereas only a weak or no cell surface staining was observed (Fig. 3.13 B). The additional permeabilisation step using a 0.1% (v/v) Triton X-100 solution gave a complete permeabilisation of cellular membranes, and the Gb3 staining was detected on the cell surface and intracellularly, apparently even in the nucleus (Fig. 3.13 C).

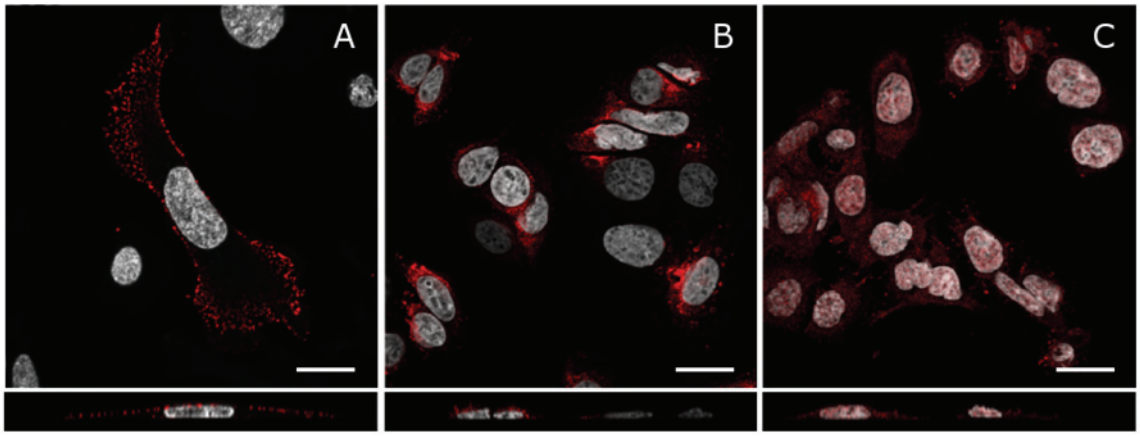

Fig. 3.13. Detection of Gb3 in SW480 cells. SW480 cells were (A) cooled on ice, (B) fixed with 10% (v/v) formalin solution or (C) fixed with 10% (v/v) formalin solution and permeabilised with 0.1% (v/v) Triton solution prior to labelling with mouse anti-Gb3, followed by rhodamine red X conjugated anti-mouse IgG (red). Nuclei were stained with (A) Hoechst 33342 (grey), or (B,C) DAPI (grey). The bottom pane shows a representative x-z section. Scale bars, 20 µm.

3.7. The relation between Gb3 and cell motility

It has been reported that the Gb3-enriched colon cancer cells are distinguished from other cells by a filopodia forming phenotype. In addition, the Gb3-enriched phenotype has been demonstrated to be closely related to cell invasiveness: the transfection of normally non-invasive epithelial cells with Gb3syn cDNA has induced the formation of filopodia and cell migration across filter membranes [8]. The SW480 cell line consists of two distinct subpopulations, which are different in their metastatic potential [78;79], and has been shown to migrate spontaneously without chemoattractive stimuli in the 3D collagen matrix [80]. Therefore, these cells were chosen for studying the relation between Gb3 and cell migration.

Firstly, several coating procedures were tested in order to have a favourable surface for cell migration (the detailed coating procedures used are explained in 2.2.6.). Two concentrations, 10 µg/cm^2 and 16 µg/cm^2 collagen, prepared either in 10 mM HCl or HEPES medium, and 1 µg/cm^2 fibronectin were tested. The results indicated that 16 µg/cm^2 concentration of collagen diluted in HEPES medium gave the best coating for the SW480 cell migration. The proportion of SW480 cells which were migrating on the dish, coated with fibronectin, 16 µg/cm^2 collagen/HCl and 16 µg/cm^2 collagen/HEPES solution, was 8%, 7% and 20%, respectively (a cell was considered migrating, if its velocity was greater than 5 µm/h) (Fig. 3.14). Therefore, the overnight coating procedure using 16 µg/cm^2 collagen diluted in HEPES medium was used for the rest of experiments.

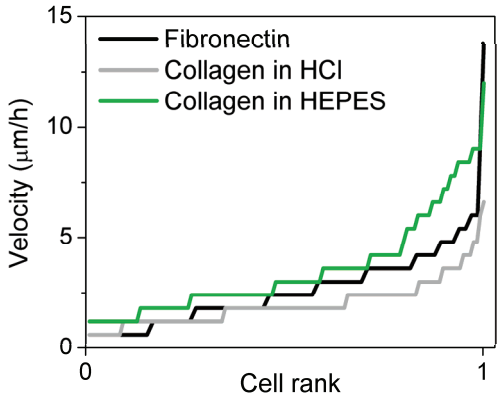

Fig. 3.14. SW480 cell migration on differently coated surfaces. The cover glass of the Petri dish (MatTek) was pre-coated with 1 µg/cm^2 fibronectin (in water), or 16 µg/cm^2 collagen, diluted in 10 mM HCl or HEPES medium. The imaging of the cells was started one day after cell seeding and proceeded for 20 h (20 min between pictures). Randomly chosen cells were tracked manually using ImageJ software and the velocity was calculated. The velocity of the cells was sorted in an ascending sequence and ranked from 0 to 1 for the plotting. The number of cells analysed for each condition, n = 65 (Fibronectin), n = 90 (Collagen in HCl), n = 109 (Collagen in HEPES).

The correlation between antibody-detected Gb3 and cell motility

SW480 cells were seeded in a collagen-coated dish one day prior to the time-lapse imaging, which lasted for 20 h. Since the Gb3 labelling was found to be highly dependent on the cell fixation and permeabilisation in SW480 cells, two different procedures for the labelling of the Gb3 were used: (i) the anti-Gb3 antibody, diluted in 37 ^{o}C complete growth medium, was added to live cells, or (ii) cells were fixed with 10% (v/v) formalin solution prior to the addition of the anti-Gb3 antibody. The permeabilisation using a 0.1% (v/v) Triton X-100 solution was performed prior to the addition of the rhodamine red X-conjugated anti-mouse IgG. The fluorescence images of the same observation points which were used for the time-lapse imaging were taken using the Biostation. The cell tracking and the analysis of the fluorescence images were performed using ImageJ software. Since SW480 cells were highly variable in their size, the measured integrated intensity of the fluorescence was divided by the cell area. The linear fitting of the data was performed using OriginPro 8.

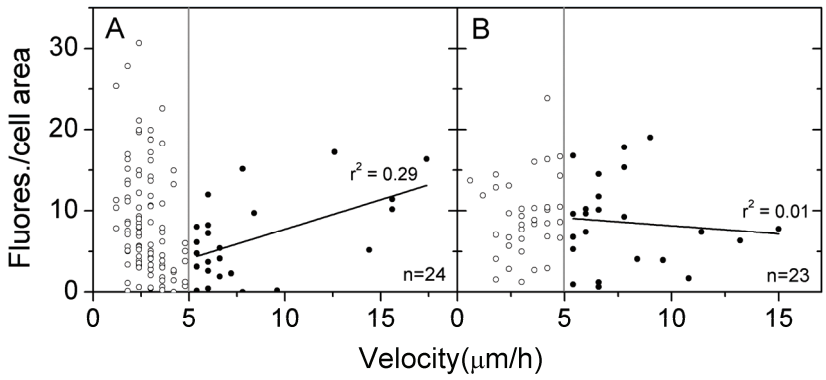

Fig. 3.15. The correlation between Gb3 and cell migration. The phase contrast images of SW480 cells were taken continuously for 20 h (20 min between pictures). (A) Anti-Gb3 was added to live cells for 30 min, or (B) cells were fixed with 10% (v/v) formalin solution prior to the addition of anti-Gb3. The cell bound/internalised anti-Gb3 was labelled with rhodamine red X-conjugated anti-mouse IgG, and fluorescence was detected using the Biostation. The cell tracking and fluorescence intensity measuring was performed using ImageJ software. The linear fitting of the data (black line) was performed only on cells which had velocity higher than 5 μm/h; r^2, coefficient of determination, calculated as a square value of correlation coefficient; n, number of cells included in the correlation analysis.

The preliminary results indicated that there was a weak correlation ($r^2 = 0.29$) between the Gb3, which was labelled by the antibody in live SW480 cells, and the velocity of the cells (Fig. 3.15 A). However, there was no correlation detected between the immunolabelled Gb3 and the cell motility in the sample, where cells were fixed with formalin prior to immunolabelling (Fig. 3.15 B). The immotile cells (velocity less than 5 μm/h) were excluded from the statistical analysis, but they were still found to have a high content of Gb3 present on the surface (Fig. 3.15 A). Therefore, further investigation is needed to elucidate the relation between the motility of the cells and the diverse expression of Gb3 on the surface.

Sodium butyrate inhibits SW480 cell motility

We have demonstrated that sodium butyrate-treated cells were sensitised to Stx, had a higher Gb3syn expression, and showed a perturbed cell proliferation. Therefore, we tested if sodium butyrate also had an effect on cell migration. SW480 cells were grown normally or with 0.5 mM or 2 mM sodium butyrate added to the complete growth medium. The growth time was 2 days (from the cell seeding until the start of the imaging), and sodium butyrate was added either immediately after the cell seeding (for 48 h incubation), or one day prior to the start of the time-lapse microscopy (for 20 h incubation). The imaging was proceeded for

20 h (with sodium butyrate still present in the medium), and then images were analysed using ImageJ software.

We found 25% cells to be motile (velocity greater than 5 μm/h) in the control group, while in sodium butyrate-treated samples, only 14% (0.5 mM butyrate treated) and 9% (2 mM butyrate treated) of the cells were found to migrate (Fig. 3.16). However, some cells were still found to migrate with the velocity as great as control cells in the sodium butyrate-treated samples. In agreement with previous results (where the data indicated that sodium butyrate interfered with the cell cycle), this suggested that the inhibitory effect on SW480 cell migration was due to cell arrest in the cell cycle phase(s) with typically lower velocity, rather than a direct effect of sodium butyrate on the cell migration.

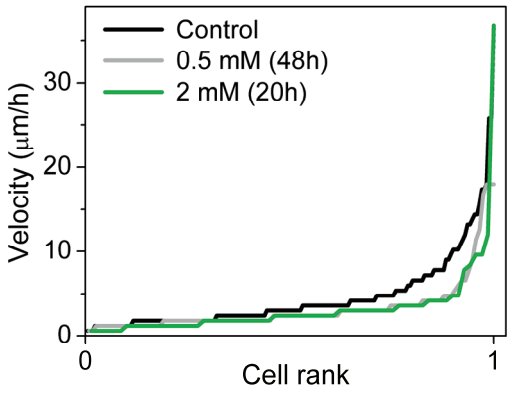

Fig. 3.16. The effect of sodium butyrate on SW480 cell migration. SW480 cells were grown normally or with 0.5 mM sodium butyrate added 48 h prior to the time-lapse imaging, or with 2 mM sodium butyrate added 20 h prior to the time-lapse imaging. Then phase contrast images of the cells were taken continuously for 20 h (20 min between pictures). The cells were tracked manually using ImageJ software and the velocity was calculated. The velocity of the cells was sorted in an ascending sequence and ranked from 0 to 1 for the plotting. The control (black line) represents data from two independent experiments (n=171), the sodium butyrate treatment experiments were performed once with n=92 (grey line) n=69 (green line) cells analysed.

Exogenously added anti-Gb3 antibody and StxB have no effect on SW480 cell motility

To test if the cross-linkage and a subsequent internalisation of the cell surface Gb3 affect the migration of SW480 cells, the motility of the cells was assessed before and after the addition of either anti-Gb3 antibodies or the B-moiety of Stx to the cells. The cells were seeded one day prior to the time-lapse imaging, and they were fed with fresh medium just before the start of imaging. The anti-Gb3 antibodies and StxB-sulf2 were added to the cells 10 h after the start of the time-lapse imaging. This addition did not disturb the cells and the focus of the microscope was not changed. Therefore, the time-lapse microscopy was performed for additional 10 h without stopping. The cells which had StxB-sulf2 added were fixed at the end of imaging, and the StxB-sulf2 was detected by the immunofluorescence. The same cell

(or a daughter cell, if the cell had divided) was tracked in the time-lapse images taken before and after the addition of the antibody or Stx-sulf2 using ImageJ software.

The results showed that the percentage of spontaneously migrating SW480 cells in the culture decreased with time, both in control and treated samples: from 47% to 34% in control, from 42% to 25% in the anti-Gb3 treated group, and from 46% to 23% in the StxB-sulf2 treated group (Fig. 3.17). The cells which had a detectable amount of StxB-sulf2 internalised were analysed separately, and the percentage of motile cells was found to decrease from 45% to 32% (Fig. 3.17. D). Though there was a slightly higher decrease observed in the proportion of migrating cells in the anti-Gb3- and StxB-sulf2-treated groups, the additional analysis of the fluorescently labelled cells did not confirm that StxB-sulf2 had an inhibitory effect on cell migration. Therefore, we concluded that neither anti-Gb3 antibodies nor StxB-sulf2 had any effect on SW480 cell motility.

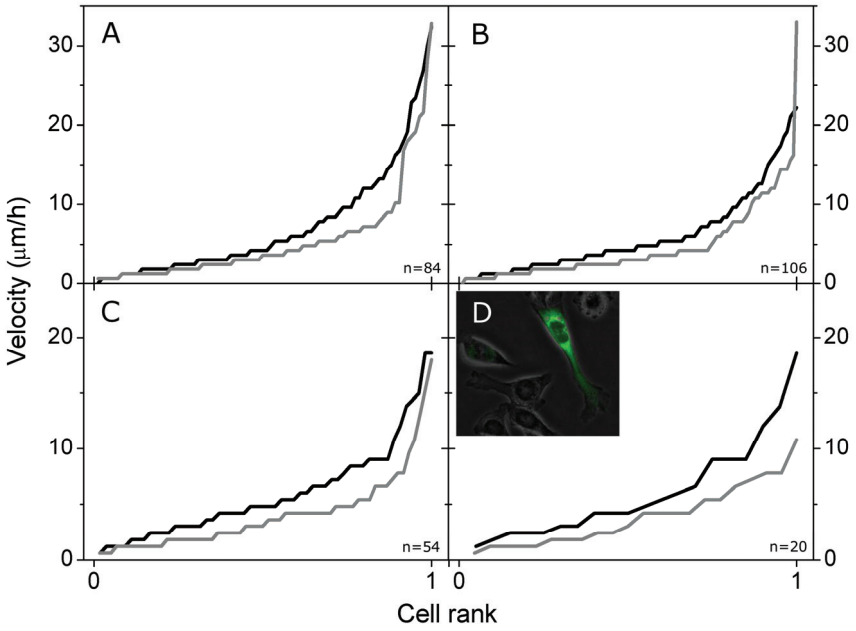

Fig. 3.17 The effect of anti-Gb3 antibody and StxB on SW480 cell migration. The phase contrast images of the cells were taken continuously for 10 h (15 min between pictures) (black line). Then (A) 20 µl sterile PBS, (B) 7 µg anti-Gb3 antibody (centrifuged and resuspended in PBS), or (C) 2.5 µg StxB-sulf2 was added, and imaging was proceeded for 10 h (grey line). (D) The StxB-sulf2-treated cells were fixed with 10% (v/v) formalin solution and permeabilised with 0.1% (v/v) Triton solution prior to labelling with mouse anti-Stx, followed by rhodamine red X-conjugated anti-mouse IgG (green) (insert). Only cells which had detectable amounts of fluorescence were included for the plotting. The velocity of the individual cells was sorted in an ascending sequence and ranked from 0 to 1 for the plotting; n, number of cells analysed.

4. Discussion

Cell context- and 2DG-induced changes in Gb3syn expression

There is still little known about the regulation of GSLs biosynthesis in cells, though, in 1971, it was first observed by Kijimoto and Hakomori [128] that Gb3syn is upregulated in response to high cell culture density in hamster fibroblasts. Moreover, it was shown that this regulation was lost after extensive passages *in vitro* or after cell transformation by polyoma virus. Therefore, it was concluded that the loss of Gb3syn regulation was related to malignant transformation of the cells [128]. However, in this study we demonstrated that cancer cell line HEp-2 increased Gb3syn expression in response to higher cell density in the culture. Moreover, we found that Gb3syn was upregulated during the course of time spent after cell seeding, even when the cells were of the same confluency. It has been suggested that biosynthesis of neutral GSLs is upregulated in response to direct cell-to-cell contact, and that GSLs are involved in cell density-dependent regulation of cell growth in normal cell cultures, but this regulation is lost during malignant transformation [128;130;135]. However, our findings show that a similar mechanism may also exist in cancer cells. Furthermore, our preliminary data indicate that Gb3syn expression may be upregulated in response to soluble factors rather than to direct cell contacts in cancer cells, since it has been found to be cell density- and time-dependent. However, additional experiments are required to characterise the mechanisms involved in Gb3 synthesis regulation in normal and cancer cells.

In agreement with earlier studies on HeLa cells [37], we found that 2DG inhibited Gb3syn expression in HEp-2 cells after short incubation times. However, there were no studies of Gb3syn expression in HeLa cells after longer 2DG treatment. Furthermore, the observed recovery of Gb3syn expression in HEp-2 cells, continuously treated with 2DG for 48 h, is in agreement with the idea that Gb3syn expression may be upregulated not only in response to direct cell-to-cell contact, but also by released soluble factors, since we showed that treated cells were inhibited in growth and did not reach high density, but still were able to increase Gb3syn expression to the same extent as control cells.

2DG-induced protection against bacterial toxins

We found that 2DG treatment induced protection against three bacterial protein toxins. As far as we know, this has not been demonstrated by any other group. We also showed that the 2DG-induced protection was not limited to a single cell line or to a single bacterial toxin, since all cell lines tested were protected against Stx, and the intoxication by three bacterial toxins, Stx, SLT-2 and DT, was decreased in HEp-2 cells after treatment with 2DG. Only the intoxication by the plant toxin ricin was found to be unaffected by 2DG treatment.

We also studied if a lowered number of Gb3 molecules could be a reason for decreased cell sensitivity to Stx after 2DG treatment, which was found to inhibit Gb3syn expression in HEp-2 cells. However, we did not observe a reduction in biotin-Stx binding and/or endocytosis after 24 h of 2DG treatment, which reduced HEp-2 sensitivity to Stx by more than 40 times. This indicates that Stx was able to enter the cells to the same extent as in control conditions, but most probably, intracellular transport of the toxin was changed and led to loss of toxicity in 2DG-treated cells. It has been shown that in cells which express Gb3, but are normally resistant to Stx, the receptor bound toxin is mainly transported to lysosomes and not detected in the ER, whereas the receptor-bound toxin is also observed in the ER in Stx sensitive cells [136]. The retrograde transport of receptor-bound Stx from endosomes to the Golgi and the ER is known to be crucial for the intoxication process (reviewed in [137]), and therefore it might be perturbed in 2DG-treated cells leading to their resistance to Stx.

The transport of Gb3-bound toxin from endosomes to the Golgi has been shown to be reduced in cells treated with PDMP (DL-threo-1-phenyl-2-decanoylamino-3-morpholino-1-propanol), which specifically inhibits the biosynthesis of hexosylceramide [110]. However, PDMP treatment did not increase the localisation of Stx in organelles positive for lysosomal marker LAMP1, and it was suggested that the toxin became trapped in endosomes or transport vesicles, which were unable to fuse with the Golgi apparatus [110]. In addition, the decreased levels of GlcCer in the cell membrane have been shown to protect cells against SLT1, and reduce the localisation of Gb3-bound toxin to detergent resistant domains (DRMs) in the membrane [138]. Multiple factors, such as length [54;87;139] and saturation [140] of fatty acids in the Gb3 molecule, a ratio between different Gb3 species [87;139], presence of other GSLs in the membrane [138], and the Gb3-bound toxin localisation within detergent resistant domains (DRMs) [141;142] have been shown to modulate the binding

and the intracellular transport of receptor-bound Stx *in vitro*. This supports the idea that although the binding of Stx is not affected by 2DG treatment, the relative composition of the Gb3 species might be changed, and thus lead to protection against the toxin. It was shown that after treatment with PDMP, the Gb3 species with short fatty acid chain (C16:0) were much faster depleted from HEp-2 cell membranes than those with long fatty acid chain (C24:1), and a three times decrease in Gb3 (C16:0) was observed even after only 4 h incubation with the drug [110]. Therefore, although there was only a small effect on total Gb3 (the majority of the Gb3 in HEp-2 cells was shown to be with long fatty acids in the structure [110]), the depletion of Gb3 with short fatty-acid chains led to a changed proportion of Gb3 species, and thus could perturb the intracellular transport of receptor-bound Stx.

However, the effect of 2DG is not completely similar to PDMP, since 2DG induces a high 20-fold protection against Stx after a rather short (4 h) incubation, while PDMP gives only a slight 1.5-fold protection in HEp-2 cells after the same incubation time [110]. The PDMP treatment does not alter the overall lipidome profile in HEp-2 cells, and specifically inhibits only the synthesis of GlcCer [110]. In contrast, 2DG interferes not only with the synthesis of Gb3, but is also known to inhibit protein N-glycosylation in the ER [143-145]. The latter could explain the protective effect against DT observed in 2DG-treated HEp-2 cells. The receptor for DT, pro-HB-EGF, is associated with membrane protein CD9/DRAP27 and heparan sulphate proteoglycans, which both have been shown to enhance DT binding to the receptor [146;147]. Since the short incubation with 2DG does not have a protective effect against DT and longer incubation time is needed to obtain the effect, this agrees with the idea that protection against DT is at least partially mediated through depletion of heparan sulphate proteoglycans. Moreover, similar protective effect against DT has been demonstrated by using tunicamycin, which also inhibits the synthesis of asparagine-linked glycoproteins [148]. Finally, we have showed that ATP depletion is not involved in 2DG-mediated protection against Stx, but may be involved in cell protection against DT, since a small, but significant rescue of sensitivity to DT was observed after addition of sodium pyruvate.

Cell sensitisation to Stx by sodium butyrate

SW480 cells were found to be less sensitive to Stx compared to HEp-2 and HT-29 cells. However, 48 h pre-treatment with sodium butyrate increased SW480 cells sensitivity to Stx by more than 80-fold, and had a much higher sensitising effect on SW480 cells than on HT-29 cells. It has been demonstrated by Sandvig *et al.* [94] that sodium butyrate induces retrograde transport of the receptor-bound Stx to the ER in A431 cells, and thereby sensitises cells to the toxin. Furthermore, it was revealed later that fatty acid chain length in the Gb3 molecules was changed in response to sodium butyrate treatment, and A431 cells, which normally expressed only short fatty acid Gb3, were found to express both long and short fatty acid Gb3 species after butyrate treatment [54].

Furthermore, we showed that sodium butyrate upregulated Gb3syn expression in colon cancer cells. This led to increased binding of biotin-Stx in HT-29 cells, suggesting an increase in Gb3 present on the cell surface. However, similarly to what had been earlier shown with other cells [54], sodium butyrate had no effect on the endocytosis of the biotin-Stx in both colon cancer cell lines tested. Interestingly, the binding of biotin-Stx was only slightly changed in SW480 cells, which were much more sensitised to Stx by sodium butyrate than HT-29 cells, suggesting that two different mechanisms might be involved in cell sensitisation to Stx after butyrate treatment in these cells. Our data indicate that HT-29 cell sensitisation to Stx can be due to a higher amount of Stx entering the cells, since the butyrate-induced upregulation of Gb3syn expression in HT-29 cells probably led to a higher number of Gb3 present on the cell surface, and therefore increased the number of cell-bound and internalized toxin. In contrast, the mechanism responsible for SW480 sensitisation to Stx by sodium butyrate seems to be different, since the increased Gb3syn activity only led to a slight increase in the total binding of biotin-Stx, and this could not explain the 80-fold sensitisation to Stx. Furthermore, unpublished data from our group indicate that there is a 2-fold increase in the total content of Gb3 after sodium butyrate treatment in SW480 cells (studied by high performance thin layer chromatography), and that there is a slight, but significant change in the ratio of short and long fatty acid Gb3, with increased proportion of long fatty acid Gb3 species in the butyrate-treated SW480 cells. Although the observed change in the proportion of Gb3 species is much lower than that shown for the A431 cells [54], it still may explain the increased cell sensitivity to Stx, since studies on model membranes, containing different proportions of long and short fatty acid Gb3 molecules,

show striking changes in the binding capacity and affinity of SLTs [87;139]. Therefore, we suggest that a change in fatty acid composition of Gb3 molecules, and not the increase in number of Gb3 available for binding, is involved in butyrate-mediated SW480 cell sensitization to Stx.

However, it is yet not clear how butyrate treatment induces the changes in fatty acid composition in the Gb3 molecules. It might be either by inducing synthesis of specific Gb3 species, or by modulating their degradation. However, the synthesis and not the degradation of Gb3 seems to be involved, since the sensitising effect of butyrate has been shown to be abolished when GSLs synthesis is inhibited in the cells [149]. There are six mammalian ceramide synthases described. They show different tissue distribution and specificity for the chain length of the FA-CoA they utilise for N-acylation of the dihydrosphingosine [150]. Thus butyrate treatment might induce the expression of a particular ceramide synthase, or change the specificity of the expressed one in a given cell. However, no published data exist describing a specific effect of butyrate on ceramide synthases.

The perturbation of the cell cycle and inhibition of cell migration by sodium butyrate

In addition to cell sensitisation to Stx and the upregulation of Gb3syn expression, we observed that sodium butyrate treatment perturbed the cytokinesis of SW480 cells and led to an increased portion of polynucleated SW480 cells in the culture. We also found that sodium butyrate treatment reduced the number of randomly migrating cells in the SW480 culture, but it had no effect on the velocity of motile cells, indicating that the reduction of the number of motile cells after sodium butyrate treatment might be due to cell accumulation in a certain phase of the cell cycle (probably G2), rather than due to a direct effect on the migratory machinery of the cell. Sodium butyrate has been shown to induce cell arrest in the G2 phase in normal and malignant cells [132;133]. Furthermore, the G2 phase has been indicated to be unfavourable for the cell migration, as shown for lymphocytes and rat carcinoma cells [151;152], and our data therefore support the idea that sodium butyrate indirectly inhibits SW480 cell migration through the cell arrest in the G2 phase of the cell cycle.

In addition, we found that binucleated SW480 cells, formed after the failed cytokinesis, were still able to reinitiate cell cycle and start a second unsuccessful cytokinesis, which led to formation of polynucleated cells. This has also been demonstrated for breast cancer cells [133] and normal fibroblasts [132], and explains the observed increase in polynucleated, but not binucleated cells in the sodium butyrate-treated SW480 cell culture. It is well known that butyrate regulates gene expression through the inhibition of histone deacetylases, which are involved in chromatin remodelling, and thus effects the expression of multiple genes. Therefore, it is not surprising that some of the key regulators of the cell cycle, such as cyclin-dependent kinases, has been shown to be affected by the sodium butyrate treatment [153;154].

The correlation between cell migration and Gb3

It has been reported that Gb3-enriched colon cancer cells are distinguished from other cells of the same culture by a filopodia forming phenotype, and have been shown to have a more invasive phenotype than cells lacking Gb3 on the surface [8]. Therefore, we studied if there was a direct correlation between Gb3 present on the cell surface and the motility of cancer cells. We found that SW480 cells were labelled with anti-Gb3 antibodies to different extents, when the labelling procedure was performed on live cells, suggesting that either some of the cells do not express Gb3, or the epitopes for antibody binding are masked in these cells. The later explanation agrees with the published data, showing that a large fraction of Gb3 might be inaccessible for the recognition by their ligands [86], because the presentation of the epitope can be modulated by cholesterol and other GSLs present in the membrane [86;134;138]. In agreement to this, we also showed that all cells in the SW480 culture were fluorescently labelled for Gb3 when cells were fixed and premeabilised prior to immunolabelling. Therefore, we have shown that all SW480 cells are expressing Gb3, but only in few of them the epitope is available for the recognition by the antibody and the B moiety of Stx.

The continuous phase contrast imaging followed by the immunolabeling of the cells allowed us to correlate the Gb3 detected by the antibody labelling to the calculated velocity of individual cells. Our preliminary data suggest that there is a correlation between Gb3 which is recognised by the antibodies and the cell velocity in the motile subpopulation of SW480 cells. Furthermore, we found no correlation between cell motility and immunolabelled Gb3

detected after cell fixation by formalin. These observations indicate that it is not the expression of Gb3 in the cells, but rather the interplay between Gb3 and other membrane components or the composition of Gb3 molecules which is related to cancer cell motility. Moreover, this could also explain, why there was no difference observed by Kovbasnjuk *et al.* [8] in the expression of Gb3syn, when Gb3-positive and Gb3-negative subpopulations of Caco-2 cells, discriminated according to their binding by StxB, were compared. Therefore, although Gb3 has been shown to be over-expressed in several cancer types [1] and has been related to colon cancer cell metastatic potential [8;86], it is becoming clear that other factors, such as the microenvironment of the membrane and the composition of Gb3 molecules, are not only regulating the function of Gb3 as a receptor for protein toxins, but also modulates the involvement of Gb3 in cancer cell motility, and thereby probably the metastases.

The insights into SW480 cell migration

SW480 cells were seeded one day (or two days in case of sodium butyrate treatment) prior to imaging in all the time-lapse experiments. However, we observed a clearly higher proportion (up to 47%) of locomoting cells when the cells were fed with fresh growth medium before the start of imaging. Only 20-25% cells were found to be locomotive in the control groups of experiments where medium was not replaced prior to the cell imaging. This observation is in agreement with published data showing that a greater proportion, up to 45% of SW480, is locomoting when monitored three hours after cell seeding, and the number of locomotive cells decreases during time, getting steady at around 25% [80]. It has been suggested that SW480 cells have a time-dependent locomotion [80], but our data imply that SW480 cell migration is dependent on growth factors (or other components) present in the growth medium, rather than time itself.

There is an ongoing discussion in the field, as to whether the assays based on cell migration on planar hard substrates can be used to mimic cell migration *in vivo,* where cells are embedded fully in soft matrix. Not surprisingly, certain migratory mechanisms have been shown to differ between the cells migrating on 2D matrixes and the cells embedded in 3D matrixes [155]. However, our observations on SW480 cell migration on the planar collagen-coated surface fully agree with the results obtained from SW480 cells migrating in 3D collagen matrix [80]. Although it is clear that some mechanisms, such as matrix remodelling are different in 2D and 3D migrating cells, we have demonstrated that planar migration-

based assays can also be a useful tool to study cell responsiveness and changes in motility within certain conditions.

The studies of this master thesis have contributed to our understanding of GSLs as important mediators in membrane dynamics. However, further investigations are required to clarify the functions of GSLs and the exact mechanisms involved in the regulation of GSL biosynthesis in normal and cancer cells.

Reference List

1. Engedal N, Skotland T, Torgersen ML, Sandvig K: **Shiga toxin and its use in targeted cancer therapy and imaging**. *Microb.Biotechnol.* 2010, **4:**32-46.

2. Ergonul Z, Clayton F, Fogo AB, Kohan DE: **Shigatoxin-1 binding and receptor expression in human kidneys do not change with age**. *Pediatr.Nephrol.* 2003, **18:**246-253.

3. Khan F, Proulx F, Lingwood CA: **Detergent-resistant globotriaosyl ceramide may define verotoxin/glomeruli-restricted hemolytic uremic syndrome pathology**. *Kidney Int.* 2009, **75:**1209-1216.

4. Lingwood CA: **Verotoxin-binding in human renal sections**. *Nephron* 1994, **66:**21-28.

5. Ohmi K, Kiyokawa N, Takeda T, Fujimoto J: **Human microvascular endothelial cells are strongly sensitive to Shiga toxins**. *Biochem.Biophys.Res.Commun.* 1998, **251:**137-141.

6. Miyamoto Y, Iimura M, Kaper JB, Torres AG, Kagnoff MF: **Role of Shiga toxin versus H7 flagellin in enterohaemorrhagic Escherichia coli signalling of human colon epithelium in vivo**. *Cell Microbiol.* 2006, **8:**869-879.

7. Cooling LL, Walker KE, Gille T, Koerner TA: **Shiga toxin binds human platelets via globotriaosylceramide (Pk antigen) and a novel platelet glycosphingolipid**. *Infect.Immun.* 1998, **66:**4355-4366.

8. Kovbasnjuk O, Mourtazina R, Baibakov B, Wang T, Elowsky C, Choti MA, Kane A, Donowitz M: **The glycosphingolipid globotriaosylceramide in the metastatic transformation of colon cancer**. *Proc.Natl.Acad.Sci.U.S.A* 2005, **102:**19087-19092.

9. Distler U, Souady J, Hulsewig M, Drmic-Hofman I, Haier J, Friedrich AW, Karch H, Senninger N, Dreisewerd K, Berkenkamp S, Schmidt MA, Peter-Katalinic J, Muthing J: **Shiga toxin receptor Gb3Cer/CD77: tumor-association and promising therapeutic target in pancreas and colon cancer**. *PloS one* 2009, **4:**e6813.

10. Alberts B, Johnson A, Lewis J, Raff m, Roberts K, Walter P: **Membrane structure. The Lipid bilayer**. In *Molecular Biology of the Cell*, edn 5. Edited by Anderson M, Granum S. New York: Garland Science; 2008:617-625.

11. van Meer G, Hoetzl S: **Sphingolipid topology and the dynamic organization and function of membrane proteins**. *FEBS lett.* 2010, **584:**1800-1805.

12. Simons K, Gerl MJ: **Revitalizing membrane rafts: new tools and insights**. *Nat.Rev.Mol.Cell Biol.* 2010, **11:**688-699.

13. The AOCS Lipid Library Internet Page. http://lipidlibrary.aocs.org/index.html/ . Date of access 3-3-2011.

14. Hannun YA, Obeid LM: **Principles of bioactive lipid signalling: lessons from sphingolipids**. *Nat.Rev.Mol.Cell Biol.* 2008, **9:**139-150.

15. Hanada K, Kumagai K, Yasuda S, Miura Y, Kawano M, Fukasawa M, Nishijima M: **Molecular machinery for non-vesicular trafficking of ceramide**. *Nature* 2003, **426:**803-809.

16. Sweeley CC: **Glycosphingolipids: structure and function**. *Pure and Appl.Chem.* 1989, **61:**1307-1312.

17. Jackson CL: **Mechanisms of transport through the Golgi complex**. *J.Cell Sci.* 2009, **122:**443-452.

18. D'Angelo G, Polishchuk E, Di Tullio G, Santoro M, Di Campli A, Godi A, West G, Bielawski J, Chuang C, van der Spoel AC, Platt FM, Hannun YA, Polishchuk R, Mattjus P, De Matteis MA: **Glycosphingolipid synthesis requires FAPP2 transfer of glucosylceramide**. *Nature* 2007, **449:**62-67.

19. Hakomori Si: **Structure and function of glycosphingolipids and sphingolipids: recollections and future trends**. *Biochim.Biophys.Acta* 2008, **1780:**325-346.

20. Hamamura K, Tsuji M, Hotta H, Ohkawa Y, Takahashi M, Shibuya H, Nakashima H, Yamauchi Y, Hashimoto N, Hattori H, Ueda M, Furukawa K, Furukawa K: **Functional activation of SRC family kinase yes is essential for the enhanced malignant properties of human melanoma cells expressing ganglioside GD3**. *J.Biol.Chem.* 2011.

21. Hakomori S: **The glycosynapse**. *Proc.Natl.Acad.Sci.U.S.A* 2002, **99:**225-232.

22. Bremer EG, Schlessinger J, Hakomori S: **Ganglioside-mediated modulation of cell growth. Specific effects of GM3 on tyrosine phosphorylation of the epidermal growth factor receptor**. *J.Biol.Chem.* 1986, **261:**2434-2440.

23. Lauvrak SU, Walchli S, Iversen TG, Slagsvold HH, Torgersen ML, Spilsberg B, Sandvig K: **Shiga toxin regulates its entry in a Syk-dependent manner**. *Mol.Biol.Cell* 2006, **17:**1096-1109.

24. Furukawa K, Okuda T, Furukawa K: **Roles of glycolipids in the development and maintenance of nervous tissues**. *Meth.Enzymol.* 2006, **417:**37-52.

25. Yamashita T, Wada R, Sasaki T, Deng C, Bierfreund U, Sandhoff K, Proia RL: **A vital role for glycosphingolipid synthesis during development and differentiation**. *Proc.Natl.Acad.Sci.U.S.A* 1999, **96:**9142-9147.

26. Proia RL: **Gangliosides help stabilize the brain**. *Nat.Genet.* 2004, **36:**1147-1148.

27. Furukawa K, Tokuda N, Okuda T, Tajima O, Furukawa K: **Glycosphingolipids in engineered mice: insights into function**. *Semin.Cell Dev.Biol.* 2004, **15:**389-396.

28. Steffensen R, Carlier K, Wiels J, Levery SB, Stroud M, Cedergren B, Nilsson SB, Bennett EP, Jersild C, Clausen H: **Cloning and expression of the histo-blood group Pk UDP-galactose: Ga1beta-4G1cbeta1-cer alpha1, 4-galactosyltransferase. Molecular genetic basis of the p phenotype**. *J.Biol.Chem.* 2000, **275:**16723-16729.

29. Mangeney M, Richard Y, Coulaud D, Tursz T, Wiels J: **CD77: an antigen of germinal center B cells entering apoptosis**. *Eur.J.Immunol.* 1991, **21:**1131-1140.

30. Clarke JT: **Narrative review: Fabry disease**. *Ann.Intern.Med.* 2007, **146:**425-433.

31. Auray-Blais C, Millington DS, barr C, Young SP, Mills K, Clarke JTR: **Letter to the Editor. Gb3/creatinine biomarkers for Fabry disease: Issue to consider**. *Mol.Genet.Metab.* 2009, **97:**237.

32. Falguieres T, Maak M, von WC, Sarr M, Sastre X, Poupon MF, Robine S, Johannes L, Janssen KP: **Human colorectal tumors and metastases express Gb3 and can be targeted by an intestinal pathogen-based delivery tool**. *Mol.Cancer Ther.* 2008, **7:**2498-2508.

33. Nudelman E, Kannagi R, Hakomori S, Parsons M, Lipinski M, Wiels J, Fellous M, Tursz T: **A glycolipid antigen associated with Burkitt lymphoma defined by a monoclonal antibody**. *Science* 1983, **220:**509-511.

34. Murray LJ, Habeshaw JA, Wiels J, Greaves MF: **Expression of Burkitt lymphoma-associated antigen (defined by the monoclonal antibody 38.13) on both normal and malignant germinal-centre B cells**. *Int.J.Cancer* 1985, **36:**561-565.

35. LaCasse EC, Saleh MT, Patterson B, Minden MD, Gariepy J: **Shiga-like toxin purges human lymphoma from bone marrow of severe combined immunodeficient mice**. *Blood* 1996, **88:**1561-1567.

36. LaCasse EC, Bray MR, Patterson B, Lim WM, Perampalam S, Radvanyi LG, Keating A, Stewart AK, Buckstein R, Sandhu JS, Miller N, Banerjee D, Singh D, Belch AR, Pilarski LM, Gariepy J: **Shiga-like toxin-1 receptor on human breast cancer, lymphoma, and myeloma and absence from CD34(+) hematopoietic stem cells: implications for ex vivo tumor purging and autologous stem cell transplantation**. *Blood* 1999, **94:**2901-2910.

37. Okuda T, Tokuda N, Numata S, Ito M, Ohta M, Kawamura K, Wiels J, Urano T, Tajima O, Furukawa K, Furukawa K: **Targeted disruption of Gb3/CD77 synthase gene resulted in the complete deletion of globo-series glycosphingolipids and loss of sensitivity to verotoxins**. *J.Biol.Chem.* 2006, **281:**10230-10235.

38. Tetaud C, Falguieres T, Carlier K, Lecluse Y, Garibal J, Coulaud D, Busson P, Steffensen R, Clausen H, Johannes L, Wiels J: **Two distinct Gb3/CD77 signaling pathways leading to apoptosis are triggered by anti-Gb3/CD77 mAb and verotoxin-1**. *J.Biol.Chem.* 2003, **278:**45200-45208.

39. Sandvig K, Torgersen ML, Engedal N, Skotland T, Iversen TG: **Protein toxins from plants and bacteria: probes for intracellular transport and tools in medicine**. *FEBS lett.* 2010, **584:**2626-2634.

40. Woodward G, Hudson M: **The effect of 2-desoxy-D-glucose on glycolysis and respiration of tumor and normal tissues**. *Cancer Res.* 1954, **14:**599-605.

41. Brown J: **Effects of 2-deoxyglucose on carbohydrate metablism: review of the literature and studies in the rat**. *Metabolism* 1962, **11:**1098-1112.

42. Maher JC, Krishan A, Lampidis TJ: **Greater cell cycle inhibition and cytotoxicity induced by 2-deoxy-D-glucose in tumor cells treated under hypoxic vs aerobic conditions**. *Cancer Chemother.Pharmacol.* 2004, **53:**116-122.

43. Khaitan D, Chandna S, Arya MB, Dwarakanath BS: **Differential mechanisms of radiosensitization by 2-deoxy-D-glucose in the monolayers and multicellular spheroids of a human glioma cell line**. *Cancer Biol.Ther.* 2006, **5:**1142-1151.

44. Zhong D, Liu X, Schafer-Hales K, Marcus AI, Khuri FR, Sun SY, Zhou W: **2-Deoxyglucose induces Akt phosphorylation via a mechanism independent of LKB1/AMP-activated protein kinase signaling activation or glycolysis inhibition**. *Mol.Cancer Ther.* 2008, **7:**809-817.

45. Okuda T, Furukawa K, Nakayama Ki: **A novel, promoter-based, target-specific assay identifies 2-deoxy-D-glucose as an inhibitor of globotriaosylceramide biosynthesis**. *FEBS J.* 2009, **276:**5191-5202.

46. Garriga-Canut M, Schoenike B, Qazi R, Bergendahl K, Daley TJ, Pfender RM, Morrison JF, Ockuly J, Stafstrom C, Sutula T, Roopra A: **2-Deoxy-D-glucose reduces epilepsy progression by NRSF-CtBP-dependent metabolic regulation of chromatin structure**. *Nat.Neurosci.* 2006, **9:**1382-1387.

47. Zhang Q, Wang SY, Fleuriel C, Leprince D, Rocheleau JV, Piston DW, Goodman RH: **Metabolic regulation of SIRT1 transcription via a HIC1:CtBP corepressor complex**. *Proc.Natl.Acad.Sci.U.S.A* 2007, **104:**829-833.

48. Kang HT, Ju JW, Cho JW, Hwang ES: **Down-regulation of Sp1 activity through modulation of O-glycosylation by treatment with a low glucose mimetic, 2-deoxyglucose**. *J.Biol.Chem.* 2003, **278:**51223-51231.

49. Scheppach W: **Effects of short chain fatty acids on gut morphology and function**. *Gut* 1994, **35:**S35-S38.

50. Augeron C, Laboisse CL: **Emergence of permanently differentiated cell clones in a human colonic cancer cell line in culture after treatment with sodium butyrate**. *Cancer Res.* 1984, **44:**3961-3969.

51. Chung YS, Song IS, Erickson RH, Sleisenger MH, Kim YS: **Effect of growth and sodium butyrate on brush border membrane-associated hydrolases in human colorectal cancer cell lines**. *Cancer Res.* 1985, **45:**2976-2982.

52. Chen TH, Chen WM, Hsu KH, Kuo CD, Hung SC: **Sodium butyrate activates ERK to regulate differentiation of mesenchymal stem cells**. *Biochem.Biophys.Res.Commun.* 2007, **355:**913-918.

53. Davie JR: **Inhibition of histone deacetylase activity by butyrate**. *J.Nutr.* 2003, **133:**2485S-2493S.

54. Sandvig K, Ryd M, Garred O, Schweda E, Holm PK, van Deurs B: **Retrograde transport from the Golgi complex to the ER of both Shiga toxin and the nontoxic Shiga B-fragment is regulated by butyric acid and cAMP**. *J.Cell Biol.* 1994, **126:**53-64.

55. Ferlay J, Parkin DM, Steliarova-Foucher E: **Estimates of cancer incidence and mortality in Europe in 2008**. *Eur.J.Cancer* 2010, **46:**765-781.

56. Talmadge JE, Fidler IJ: **AACR centennial series: the biology of cancer metastasis: historical perspective**. *Cancer Res.* 2010, **70:**5649-5669.

57. Yilmaz M, Christofori G: **Mechanisms of motility in metastasizing cells**. *Mol.Cancer Res.* 2010, **8:**629-642.

58. Friedl P, Wolf K: **Plasticity of cell migration: a multiscale tuning model**. *J.Cell Biol.* 2010, **188:**11-19.

59. Sabeh F, Shimizu-Hirota R, Weiss SJ: **Protease-dependent versus -independent cancer cell invasion programs: three-dimensional amoeboid movement revisited**. *J.Cell Biol.* 2009, **185:**11-19.

60. Thiery JP, Sleeman JP: **Complex networks orchestrate epithelial-mesenchymal transitions**. *Nat.Rev.Mol.Cell Biol.* 2006, **7:**131-142.

61. Wheelock MJ, Shintani Y, Maeda M, Fukumoto Y, Johnson KR: **Cadherin switching**. *J.Cell Sci.* 2008, **121:**727-735.

62. Suyama K, Shapiro I, Guttman M, Hazan RB: **A signaling pathway leading to metastasis is controlled by N-cadherin and the FGF receptor**. *Cancer Cell* 2002, **2:**301-314.

63. Ridley AJ: **Rho GTPases and actin dynamics in membrane protrusions and vesicle trafficking**. *Trends Cell Biol.* 2006, **16:**522-529.

64. Takeichi M: **Cadherin cell adhesion receptors as a morphogenetic regulator**. *Science* 1991, **251:**1451-1455.

65. Hynes RO: **Integrins: versatility, modulation, and signaling in cell adhesion**. *Cell* 1992, **69:**11-25.

66. Hakomori S: **Glycosylation defining cancer malignancy: new wine in an old bottle**. *Proc.Natl.Acad.Sci.U.S.A* 2002, **99:**10231-10233.

67. Hakomori S, Nudelman E, Levery SB, Kannagi R: **Novel fucolipids accumulating in human adenocarcinoma. I. Glycolipids with di- or trifucosylated type 2 chain**. *J.Biol.Chem.* 1984, **259:**4672-4680.

68. Ladisch S, Sweeley CC, Becker H, Gage D: **Aberrant fatty acyl alpha-hydroxylation in human neuroblastoma tumor gangliosides**. *J.Biol.Chem.* 1989, **264:**12097-12105.

69. Ohyama C, Fukushi Y, Satoh M, Saitoh S, Orikasa S, Nudelman E, Straud M, Hakomori S: **Changes in glycolipid expression in human testicular tumor**. *Int.J.Cancer* 1990, **45:**1040-1044.

70. Cooling LL, Zhang DS, Naides SJ, Koerner TA: **Glycosphingolipid expression in acute nonlymphocytic leukemia: common expression of shiga toxin and parvovirus B19 receptors on early myeloblasts**. *Blood* 2003, **101:**711-721.

71. Portoukalian J, Zwingelstein G, Dore JF: **Lipid composition of human malignant melanoma tumors at various levels of malignant growth**. *Eur.J.Biochem.* 1979, **94:**19-23.

72. Carubia JM, Yu RK, Macala LJ, Kirkwood JM, Varga JM: **Gangliosides of normal and neoplastic human melanocytes**. *Biochem.Biophys.Res.Commun.* 1984, **120:**500-504.

73. Kawamura S, Ohyama C, Watanabe R, Satoh M, Saito S, Hoshi S, Gasa S, Orikasa S: **Glycolipid composition in bladder tumor: a crucial role of GM3 ganglioside in tumor invasion**. *Int.J.Cancer* 2001, **94:**343-347.

74. Miura Y, Kainuma M, Jiang H, Velasco H, Vogt PK, Hakomori S: **Reversion of the Jun-induced oncogenic phenotype by enhanced synthesis of sialosyllactosylceramide (GM3 ganglioside)**. *Proc.Natl.Acad.Sci.U.S.A* 2004, **101:**16204-16209.

75. Mora PT, Fishman PH, Bassin RH, Brady RO, McFarland VW: **Transformation of Swiss 3T3 cells by murine sarcoma virus is followed by decrease in a glycolipid glycosyltransferase**. *Nat.New Biol.* 1973, **245:**226-229.

76. Bai H, Orlando J, Seyfried TN: **Altered ganglioside composition in virally transformed rat embryo fibroblasts**. *Biochim.Biophys.Acta* 1992, **1136:**23-27.

77. Leibovitz A, Stinson JC, McCombs WB, III, McCoy CE, Mazur KC, Mabry ND: **Classification of human colorectal adenocarcinoma cell lines**. *Cancer Res.* 1976, **36:**4562-4569.

78. Tomita N, Jiang W, Hibshoosh H, Warburton D, Kahn SM, Weinstein IB: **Isolation and characterization of a highly malignant variant of the SW480 human colon cancer cell line**. *Cancer Res.* 1992, **52:**6840-6847.

79. Yoon W-H, Lee S-K, Song K-S, Kim J-S, Kim T-D, Li G, Yun E-J, Heo J-Y, Jung Y-J, Park J-I, Kweon G-R, Koo S-H, Park H-D, Hwang B-D, Lim K: **The tumorigenic, invasive and metastatic potential of epithelial and round subpopulations of the SW480 human colon cancer cell line**. *Mol.Med.Report* 2008, **1:**763-768.

80. Kubens BS, Zanker KS: **Differences in the migration capacity of primary human colon carcinoma cells (SW480) and their lymph node metastatic derivatives (SW620)**. *Cancer Lett.* 1998, **131:**55-64.

81. Product Catalog, HTB-38. American Type Culture Collection (ATCC). https://www.lgcstandards-atcc.org/ . Date of access 5-8-2010.

82. Johannes L, Romer W: **Shiga toxin: from cell biology to biomedical applications**. *Nat.Rev.Microbiol.* 2010, **8:**105-116.

83. Ling H, Boodhoo A, Hazes B, Cummings MD, Armstrong GD, Brunton JL, Read RJ: **Structure of the shiga-like toxin I B-pentamer complexed with an analogue of its receptor Gb3**. *Biochemistry* 1998, **37:**1777-1788.

84. Soltyk AM, MacKenzie CR, Wolski VM, Hirama T, Kitov PI, Bundle DR, Brunton JL: **A mutational analysis of the globotriaosylceramide-binding sites of verotoxin VT1**. *J.Biol.Chem.* 2002, **277:**5351-5359.

85. Windschiegl B, Orth A, Romer W, Berland L, Stechmann B, Bassereau P, Johannes L, Steinem C: **Lipid reorganization induced by Shiga toxin clustering on planar membranes**. *PloS one* 2009, **4:**e6238.

86. Mahfoud R, Manis A, Binnington B, Ackerley C, Lingwood CA: **A major fraction of glycosphingolipids in model and cellular cholesterol-containing membranes is undetectable by their binding proteins**. *J.Biol.Chem.* 2010, **285:**36049-36059.

87. Pellizzari A, Pang H, Lingwood CA: **Binding of verocytotoxin 1 to its receptor is influenced by differences in receptor fatty acid content**. *Biochemistry* 1992, **31:**1363-1370.

88. Head SC, Karmali MA, Lingwood CA: **Preparation of VT1 and VT2 hybrid toxins from their purified dissociated subunits. Evidence for B subunit modulation of a subunit function**. *J.Biol.Chem.* 1991, **266:**3617-3621.

89. Tesh VL, Burris JA, Owens JW, Gordon VM, Wadolkowski EA, O'Brien AD, Samuel JE: **Comparison of the relative toxicities of Shiga-like toxins type I and type II for mice**. *Infect.Immun.* 1993, **61:**3392-3402.

90. Siegler RL, Obrig TG, Pysher TJ, Tesh VL, Denkers ND, Taylor FB: **Response to Shiga toxin 1 and 2 in a baboon model of hemolytic uremic syndrome**. *Pediatr.Nephrol.* 2003, **18:**92-96.

91. Boerlin P, McEwen SA, Boerlin-Petzold F, Wilson JB, Johnson RP, Gyles CL: **Associations between virulence factors of Shiga toxin-producing Escherichia coli and disease in humans**. *J.Clin.Microbiol.* 1999, **37:**497-503.

92. Palermo MS, Exeni RA, Fernandez GC: **Hemolytic uremic syndrome: pathogenesis and update of interventions**. *Expert.Rev.Anti.Infect.Ther.* 2009, **7:**697-707.

93. Marcato P, Mulvey G, Armstrong GD: **Cloned Shiga toxin 2 B subunit induces apoptosis in Ramos Burkitt's lymphoma B cells**. *Infect.Immun.* 2002, **70:**1279-1286.

94. Sandvig K, Garred O, Prydz K, Kozlov JV, Hansen SH, van DB: **Retrograde transport of endocytosed Shiga toxin to the endoplasmic reticulum**. *Nature* 1992, **358:**510-512.

95. Sandvig K, van Deurs B: **Delivery into cells: lessons learned from plant and bacterial toxins**. *Gene Ther.* 2005, **12:**865-872.

96. Oram DM, Holmes Randall K: **Diphtheria toxin**. In *The Comprehensive Sourcebook of Bacterial Protein Toxins*, edn 3rd. Edited by Alouf J, Popoff M. Elsevier Ltd; 2006:245-256.

97. Naglich JG, Metherall JE, Russell DW, Eidels L: **Expression cloning of a diphtheria toxin receptor: identity with a heparin-binding EGF-like growth factor precursor**. *Cell* 1992, **69:**1051-1061.

98. Simpson JC, Smith DC, Roberts LM, Lord JM: **Expression of mutant dynamin protects cells against diphtheria toxin but not against ricin**. *Exp.Cell Res.* 1998, **239:**293-300.

99. Gordon VM, Klimpel KR, Arora N, Henderson MA, Leppla SH: **Proteolytic activation of bacterial toxins by eukaryotic cells is performed by furin and by additional cellular proteases**. *Infect.Immun.* 1995, **63:**82-87.

100. Wang J, London E: **The membrane topography of the diphtheria toxin T domain linked to the a chain reveals a transient transmembrane hairpin and potential translocation mechanisms**. *Biochemistry* 2009, **48:**10446-10456.

101. Blewitt MG, Chung LA, London E: **Effect of pH on the conformation of diphtheria toxin and its implications for membrane penetration**. *Biochemistry* 1985, **24:**5458-5464.

102. Sandvig K, Olsnes S: **Diphtheria toxin entry into cells is facilitated by low pH**. *J.Cell Biol.* 1980, **87:**828-832.

103. Falnes PO, Sandvig K: **Penetration of protein toxins into cells**. *Curr.Opin.Cell Biol.* 2000, **12:**407-413.

104. Honjo T, Nishizuka Y, Hayaishi O: **Diphtheria toxin-dependent adenosine diphosphate ribosylation of aminoacyl transferase II and inhibition of protein synthesis**. *J.Biol.Chem.* 1968, **243:**3553-3555.

105. Gill DM, Pappenheimer AM, Jr., Brown R, Kurnick JT: **Studies on the mode of action of diphtheria toxin. VII. Toxin-stimulated hydrolysis of nicotinamide adenine dinucleotide in mammalian cell extracts**. *J.Exp.Med.* 1969, **129:**1-21.

106. Olsnes S, Kozlov JV: **Ricin**. *Toxicon* 2001, **39:**1723-1728.

107. Rutenber E, Katzin BJ, Ernst S, Collins EJ, Mlsna D, Ready MP, Robertus JD: **Crystallographic refinement of ricin to 2.5 A**. *Proteins* 1991, **10:**240-250.

108. Olsnes S: **The history of ricin, abrin and related toxins**. *Toxicon* 2004, **44:**361-370.

109. Grimmer S, Spilsberg B, Hanada K, Sandvig K: **Depletion of sphingolipids facilitates endosome to Golgi transport of ricin**. *Traffic* 2006, **7:**1243-1253.

110. Raa H, Grimmer S, Schwudke D, Bergan J, Walchli S, Skotland T, Shevchenko A, Sandvig K: **Glycosphingolipid requirements for endosome-to-Golgi transport of Shiga toxin**. *Traffic* 2009, **10:**868-882.

111. Rodal SK, Skretting G, Garred O, Vilhardt F, van DB, Sandvig K: **Extraction of cholesterol with methyl-beta-cyclodextrin perturbs formation of clathrin-coated endocytic vesicles**. *Mol.Biol.Cell* 1999, **10:**961-974.

112. Rapak A, Falnes PO, Olsnes S: **Retrograde transport of mutant ricin to the endoplasmic reticulum with subsequent translocation to cytosol**. *Proc.Natl.Acad.Sci.U.S.A* 1997, **94:**3783-3788.

113. Sandvig K, van Deurs B: **Membrane traffic exploited by protein toxins**. *Annu.Rev.Cell Dev.Biol.* 2002, **18:**1-24.

114. Endo Y, Tsurugi K: **RNA N-glycosidase activity of ricin A-chain. Mechanism of action of the toxic lectin ricin on eukaryotic ribosomes**. *J.Biol.Chem.* 1987, **262:**8128-8130.

115. Aktories K: **Toxins as tools**. In *The Comprehensive Sourcebook of Bacterial Protein Toxins*, edn 3rd. Edited by Alouf J, Popoff M. Elsevier Ltd; 2006:976-990.

116. Eklund JW, Kuzel TM: **Denileukin diftitox: a concise clinical review**. *Expert.Rev.Anticancer Ther.* 2005, **5:**33-38.

117. Prier A, Chenal A, Babon A, Menez A, Gillet D: **Engineering of bacterial toxins for research and medicine**. In *The Comprehensive Sourcebook of Bacterial Protein Toxins*, edn 3rd. Edited by Alouf J, Popoff M. Elsevier Ltd; 2006:991-1007.

118. Potala S, Sahoo SK, Verma RS: **Targeted therapy of cancer using diphtheria toxin-derived immunotoxins**. *Drug Discov.Today* 2008, **13:**807-815.

119. Choudhary S, Mathew M, Verma RS: **Therapeutic potential of anticancer immunotoxins**. *Drug Discov.Today* 2011, **Article in Press, Uncorrected Proof**.

120. Viel T, Dransart E, Nemati F, Henry E, Theze B, Decaudin D, Lewandowski D, Boisgard R, Johannes L, Tavitian B: **In vivo tumor targeting by the B-subunit of shiga toxin**. *Mol.Imaging* 2008, **7:**239-247.

121. Moore A, Sabachewsky L, Toolan H: **Culture characteristics of four permanent lines of human cancer cells**. *Cancer Res.* 1955, **15:**598-602.

122. Product Catalog, CCL-23. American Type Culture Collection (ATCC). https://www.lgcstandards-atcc.org/ . Date of access 5-8-2010.

123. Product Catalog, CCL-228. American Type Culture Collection (ATCC). https://www.lgcstandards-atcc.org/ . Date of access 5-8-2010.

124. Product Catalog, HTB-38. American Type Culture Collection (ATCC). https://www.lgcstandards-atcc.org/ . Date of access 5-8-2010.

125. Molecular Station Internet page. http://www.molecularstation.com/ . Date of access 6-8-2010.

126. M-SERIES® M1R Analyzer User Guide. 2004. Gaithersburg, Maryland, USA, BioVeris Corporation.

127. Electronic Statistics Textbook. Tulsa, OK: StatSoft. http://www.statsoft.com/textbook . Date of access 10-5-2011.

128. Kijimoto S, Hakomori S: **Enhanced glycolipid: á-galactosyltransferase activity in contact-inhibited hamster cells, and loss of this response in polyoma transformants**. *Biochem.Biophys.Res.Commun.* 1971, **44:**557-563.

129. Chung SJ, Lee SH, Lee YJ, Park HS, Bunger R, Kang YH: **Pyruvate protection against endothelial cytotoxicity induced by blockade of glucose uptake**. *J.Biochem.Mol.Biol.* 2004, **37:**239-245.

130. Hakomori S: **Cell density-dependent changes of glycolipid concentrations in fibroblasts, and loss of this response in virus-transformed cells**. *Proc.Natl.Acad.Sci.U.S.A* 1970, **67:**1741-1747.

131. Larsen JK, Christensen IJ, Kieler J: **Cell cycle perturbation by sodium butyrate in tumorigenic and non-tumorigenic human urothelial cell lines assessed by flow cytometric bromodeoxyuridine/DNA analysis**. *Cell Prolif.* 1995, **28:**359-371.

132. Yamada K, Kimura G: **Formation of proliferative tetraploid cells after treatment of diploid cells with sodium butyrate in rat 3Y1 fibroblasts**. *J.Cell Physiol* 1985, **122:**59-63.

133. Lallemand F, Courilleau D, Buquet-Fagot C, Atfi A, Montagne MN, Mester J: **Sodium butyrate induces G2 arrest in the human breast cancer cells MDA-MB-231 and renders them competent for DNA rereplication**. *Exp.Cell Res.* 1999, **247:**432-440.

134. Lingwood D, Binnington B, Rog T, Vattulainen I, Grzybek M, Coskun U, Lingwood CA, Simons K: **Cholesterol modulates glycolipid conformation and receptor activity**. *Nat.Chem.Biol.* 2011, **7:**260-262.

135. Vukelic Z, Kalanj-Bognar S: **Cell density-dependent changes of glycosphingolipid biosynthesis in cultured human skin fibroblasts**. *Glycoconj.J.* 2001, **18:**429-437.

136. Hoey DE, Sharp L, Currie C, Lingwood CA, Gally DL, Smith DG: **Verotoxin 1 binding to intestinal crypt epithelial cells results in localization to lysosomes and abrogation of toxicity**. *Cell Microbiol.* 2003, **5:**85-97.

137. Sandvig K, Bergan J, Dyve AB, Skotland T, Torgersen ML: **Endocytosis and retrograde transport of Shiga toxin**. *Toxicon* 2009,1-5.

138. Smith DC, Sillence DJ, Falguieres T, Jarvis RM, Johannes L, Lord JM, Platt FM, Roberts LM: **The association of Shiga-like toxin with detergent-resistant membranes is modulated by glucosylceramide and is an essential requirement in the endoplasmic reticulum for a cytotoxic effect**. *Mol.Biol.Cell* 2006, **17:**1375-1387.

139. Mahfoud R, Manis A, Lingwood CA: **Fatty acid-dependent globotriaosyl ceramide receptor function in detergent resistant model membranes**. *J.Lipid Res.* 2009, **50:**1744-1755.

140. Kiarash A, Boyd B, Lingwood CA: **Glycosphingolipid receptor function is modified by fatty acid content. Verotoxin 1 and verotoxin 2c preferentially recognize different globotriaosyl ceramide fatty acid homologues**. *J.Biol.Chem.* 1994, **269:**11138-11146.

141. Falguieres T, Mallard F, Baron C, Hanau D, Lingwood C, Goud B, Salamero J, Johannes L: **Targeting of Shiga toxin B-subunit to retrograde transport route in association with detergent-resistant membranes**. *Mol.Biol.Cell* 2001, **12:**2453-2468.

142. Falguieres T, Romer W, Amessou M, Afonso C, Wolf C, Tabet JC, Lamaze C, Johannes L: **Functionally different pools of Shiga toxin receptor, globotriaosyl ceramide, in HeLa cells**. *FEBS J.* 2006, **273:**5205-5218.

143. Datema R, Schwarz RT: **Formation of 2-Deoxyglucose-Containing Lipid-Linked Oligosaccharides. Interference with Glycosylation of Glycoproteins**. *Eur.J.Biochem.* 1978, **90:**505-516.

144. Kurtoglu M, Maher JC, Lampidis TJ: **Differential toxic mechanisms of 2-deoxy-D-glucose versus 2-fluorodeoxy-D-glucose in hypoxic and normoxic tumor cells**. *Antioxid.Redox.Signal* 2007, **9:**1383-1390.

145. Merchan JR, Kovacs K, Railsback JW, Kurtoglu M, Jing Y, Pina Y, Gao N, Murray TG, Lehrman MA, Lampidis TJ: **Antiangiogenic activity of 2-deoxy-D-glucose**. *PloS one* 2010, **5:**e13699.

146. Shishido Y, Sharma KD, Higashiyama S, Klagsbrun M, Mekada E: **Heparin-like molecules on the cell surface potentiate binding of diphtheria toxin to the diphtheria toxin receptor/membrane-anchored heparin-binding epidermal growth factor-like growth factor**. *J.Biol.Chem.* 1995, **270:**29578-29585.

147. Mitamura T, Iwamoto R, Umata T, Yomo T, Urabe I, Tsuneoka M, Mekada E: **The 27-kD diphtheria toxin receptor-associated protein (DRAP27) from vero cells is the monkey homologue of human CD9 antigen: expression of DRAP27 elevates the number of diphtheria toxin receptors on toxin-sensitive cells**. *J.Cell Biol.* 1992, **118:**1389-1399.

148. Hranitzky KW, Durham DL, Hart DA, Eidels L: **Role of glycosylation in expression of functional diphtheria toxin receptors**. *Infect.Immun.* 1985, **49:**336-343.

149. Sandvig K, Garred O, van Helvoort A, van Meer G, van Deurs B: **Importance of glycolipid synthesis for butyric acid-induced sensitization to shiga toxin and intracellular sorting of toxin in A431 cells**. *Mol.Biol.Cell* 1996, **7:**1391-1404.

150. Stiban J, Tidhar R, Futerman AH: **Ceramide synthases: Roles in cell Physiology and Signaling**. In *Sphingolipids as Signaling and Regulatory Molecules*. Edited by Chalfant C, Del Poeta M. Landes Bioscience; 2010.

151. Bonneton C, Sibarita JB, Thiery JP: **Relationship between cell migration and cell cycle during the initiation of epithelial to fibroblastoid transition**. *Cell Motil.Cytoskeleton* 1999, **43:**288-295.

152. Masuyama J, Berman JS, Cruikshank WW, Morimoto C, Center DM: **Evidence for recent as well as long term activation of T cells migrating through endothelial cell monolayers in vitro**. *J.Immunol.* 1992, **148:**1367-1374.

153. Li CJ, Li RW: **Butyrate induced cell cycle arrest in bovine cells through targeting gene expression relevant to DNA replication apparatus**. *Gene Regul.Syst.Bio* 2008, **2:**113-123.

154. Charollais RH, Buquet C, Mester J: **Butyrate blocks the accumulation of CDC2 mRNA in late G1 phase but inhibits both the early and late G1 progression in chemically transformed mouse fibroblasts BP-A31**. *J.Cell Physiol* 1990, **145:**46-52.

155. Fraley SI, Feng Y, Krishnamurthy R, Kim DH, Celedon A, Longmore GD, Wirtz D: **A distinctive role for focal adhesion proteins in three-dimensional cell motility**. *Nat.Cell Biol.* 2010, **12:**598-604.

Appendix

Reagents used in this study:

Product name	Supplier	Cat. No.
10% formalin solution	Sigma	HT5014
2-deoxy-D-glucose	Sigma	D6134
BSA (bovine serum albumin)	Sigma	A7888
$CaCl_2 \cdot 2H_2O$	Merck Chemicals	156182
Collagen, rat tail, type I	BD Bioscience	354249
cOmplete EDTA-free Protease Inhibitor Cocktail Tablets	Roche	04 693 132 001
DMEM growth medium	Invitrogen	41965
DMEM/F12 growth medium	Invitrogen	11320
Dynabeads M-280 Streptavidin	Invitrogen	112-06D
EDTA, disodium salt	Merck Chemicals	324503
Emulsifier-Safe™	PerkinElmer	6013389
EZ-Link Sulfo-NHS-SS-Biotin	Pierce Biotechnology	21331
FBS (fetal bovine serum)	Sigma	F7524
Fibronectin	Sigma	F2006
HEPES	BDH Chemicals	4414767
Hoechst 33342	Sigma	B2261
ISOTON II diluent	Beckman Coulter	8546719
KCl	Merck Chemicals	529552
KH_2PO_4	Merck Chemicals	529568
L-[3,4,5-^{3}H(N)]-leucine	PerkinElmer	NET460005MC
L-glutamine solution	Invitrogen	25030
MEM (minimal essential medium)	Invitrogen	22600134

MEM (minimal essential medium without leucine)	Invitrogen	11890
MESNa (sodium 2-mercaptoethanesulfonate)	Sigma	M1511
$Na_2HPO_4 \cdot 12H_2O$	Merck Chemicals	106579
$Na_2HPO_4 \cdot 2H_2O$	Merck Chemicals	106580
NaCl	Merck Chemicals	106404
$NaH_2PO_4 \cdot 2H_2O$	Merck Chemicals	106346
NaOH	Merck Chemicals	567530
Octyl β-D-glucopyranoside	Sigma	O8001
Penicillin/streptomycin solution	Invitrogen	15140
ProLong Gold antifade reagent with DAPI	Invitrogen	P-36931
RNase-free (DEPC treated) water	Invitrogen	75-0024
RPMI 1640 growth medium	Invitrogen	21875
TritonX-100	Sigma	T9284
Tween-20	Sigma	P1379
β-mercaptoethanol	Sigma	63689

HEPES medium

Reagent	Amount	Final concentration
MEM (minimum essential medium)	1 pack	-
HEPES	47.7 g	20 mM
L-glutamine solution	100 ml	2 mM
Penicillin/streptomycin solution	100 ml	100 U/ml – penicillin 100 μg/ml - streptomycin
Distilled water	10 l	-

Adjusted with NaOH to pH 7.7. Sterile filtered and stored at + 4 ^{o}C.

Leucine-free medium

Reagent	Amount	Final concentration
MEM without leucine	80 g	-
HEPES	44.7 g	20 mM
L-glutamine solution	100 ml	2 mM
Penicillin/streptomycin solution	100 ml	100 U/ml – penicillin 100 μg/ml - streptomycin
Distilled water	10 l	-

Adjusted with NaOH to pH 7.7. Sterile filtered and stored at + 4 ^{o}C.

Complete growth medium

Reagent/Solution	Amount	Final concentration
Medium (DMEM, DMEM/F12 or RPMI 1640)	440 ml	-
Fetal bovine serum (FBS)	50 ml	10% (v/v)
L-glutamine solution	5 ml	2 mM
Penicillin/streptomycin solution	5 ml	100 U/ml – penicillin 100 μg/ml - streptomycin

Stored at + 4 ^{o}C.

Trypsin/EDTA solution

Reagent	Amount	Final concentration
KCl	4.0 g	5.4 mM
NaCl	80 g	0.14 M
Glucose	10 g	5.6 mM
Phenol Red	0.10 g	28 μM
$NaHCO_3$	3.5 g	4.2 mM
Trypsin	5.0 g	0.05% (w/v)
EDTA	2.0 g	0.54 mM
Penicillin/streptomycin solution	100 ml	100 U/ml – penicillin 100 μg/ml - streptomycin
Distilled water	10 l	-

Adjusted with NaOH to pH 7.6. Sterile filtered and stored at + 4 ^{o}C.

Phosphate buffered saline (PBS)

Reagent	Amount	Final concentration
$NaH_2PO_4 \cdot 2H_2O$	0.16 g	1.0 mM
$Na_2HPO_4 \cdot 12H_2O$	1.98 g	5.5 mM
NaCl	8.1 g	0.14 M
Distilled water	1 l	-

Adjusted with NaOH to pH 7.5. Stored at + 4 ^{o}C.

HEPES buffer

Reagent	Amount	Final concentration
$CaCl_2 \cdot 2H_2O$	3.16 g	5.4 mM
HEPES	19.08 g	20 mM
NaCl	32.76 g	0.14 M
Distilled water	4 l	-

Adjusted with NaOH to pH 7.0. Stored at + 4 ^{o}C.

Lysis buffer

Reagent	Amount	Final concentration
NaCl	2.92 g	0.1 M
$Na_2HPO_4 \cdot 2H_2O$	0.89 g	10 mM
EDTA	0.19 g	1 mM
Triton X-100	5 ml	1% (v/v)
Distilled water	up to 500 ml	-

Adjusted with NaOH to pH 7.4. Stored at + 4 ^{o}C.

Cell lysis solution

Reagent/Solution	Amount
Lysis buffer	4.8 ml
cOmplete EDTA-free Protease Inhibitor Cocktail Tablets	1/10 of a tablet (dissolved in distilled water and kept frozen before usage)
Octyl β-D-glucopyranoside	0.085 g

Freshly made at the same day of experiment and kept at + 4 ^{o}C.

Lysis buffer – Rneasy Plus Mini Kit for RNA isolation

Reagent/Solution	Amount
Buffer RLT Plus	5 ml
β-mercaptoethanol	50 µl

Shelf life of 1 month.

MESNa solution

Reagent	Final concentration
Sodium 2-mercaptoethanesulfonate (MESNa)	0.1 M
Bovine serum albumin (BSA)	2 mg/ml
HEPES buffer pH 8.6	(Prepared only as much as needed for the current experiment)

Freshly made at the same day of experiment and kept at + 4 ^{o}C.

Assay diluent for biotin-Stx endocytosis assay

Reagent	Amount	Final concentration
Bovine serum albumin (BSA) (10 mg/ml stock in PBS)	4 ml	0.2% (w/v)
Tween-20	100 µl	0.5% (v/v)
PBS	up to 20 ml	-

Freshly made just before use.